

Advances in 2D Based Field Effect Transistors as Biosensing Platforms: From Principle to Biomedical Applications

Foad Ghasemi^{1*}, Abdollah Salimi^{2,3*}

¹Nanoscale Physics Device Lab (NPDL), Department of Physics, University of Kurdistan, 66177-15175, Sanandaj, Iran.

²Department of Chemistry, University of Kurdistan, 66177-15175, Sanandaj-Iran.

³Research Center for Nanotechnology, University of Kurdistan, 66177-15175, Sanandaj-Iran.

*Corresponding Authors

f.ghasemi@uok.ac.ir, absalimi@uok.ac.ir,

Abstract:

Two-dimensional (2D) materials have been used extensively in various fields due to their unique physical and chemical properties. Among their diverse applications, field-effect transistor biosensors (bio-FETs) promise a brilliant prospect in the fabrication of biodevices for diagnostics especially point of care (PoC) based biomedical testing. The introduction of 2D nanomaterials as a sensing platform not only promotes their bioassay process but also provides label-free, low-cost, real-time, highly sensitive, and selective detection of different biomolecules. 2D-based bio-FETs are highly desirable for biosensing applications due to large effective surface area, environment-dependent conductivity, being easily functionalized, biocompatible and simple fabrication processes. This review focuses comprehensively on 2D bio-FETs and more on both dry and wet states. In this regard, these bio-FETs are classified into four categories including Apta, DNA (Geno), Immuno, and enzymatic biosensors. The configuration, detection mechanism and electrical signal processing of each category are discussed in response to different biotargets. Finally, their promising roles as PoC testing devices for modern medicine are discussed in biomedical (real) samples.

Keywords: 2D materials, FET biosensors, Aptamer, DNA, Immuno, Enzymatic, Point of Care, Clinical samples.

1. Introduction

Human health is a critical key to the continuity of life, which attempts to improve it resulting in an increase in life quality [1]. Several factors can endanger human health, the most important of them are diseases [2]. As a result, the diagnostic and treatment of diseases play essential roles in protecting human health[3]. Until now, various methods have been introduced to diagnose diseases such as: chemical testing [4], medical imaging [5], spectroscopic techniques [6], electrodiagnostic medicine [7], DNA testing [8], visual examination [9], and physical examination [10]. Observational or physical methods usually come with less accuracy and in special cases, more advanced imaging or spectroscopic techniques are required [11]. However, these methods are time-consuming, labor intensive, high cost, and in some cases associated with low sensitivities [12, 13]. Therefore, significant efforts are ongoing to introduce effective, efficient and inexpensive medical methods.

In the last decade, biosensors demonstrate a superior candidate for disease diagnostic purposes. A biosensor is defined as an analytical device consisting of detector and biomolecule recognition components [14]. The latter part is served to interact with the target analyst and the detector converts the biological response into the desired signals [14]. Based on detection mechanism, biosensors categorize into electrochemical, fluorescent, colorimetric, field effect transistor (FET), surface plasmon resonance (SPR), and piezoelectric biosensors [15-18]. They can recognize various biomolecules including enzymes, carbohydrates (glucose, uric acid, lactic acid), lipids (Cholesterol), proteins, antibodies, viruses, bacteria, and nucleic acids (RNA, DNA) [19-24]. However, practical applications of some biosensors are limited due to lack of selectivity, low stability, and being as expensive devices [25-28].

Among them, FET biosensors have attracted considerable attention because they not only promise sensitive, selective, label-free, early, and fast detection of biomolecules, but also are compatible with silicon industry [29-32]. A FET biosensor is composed of a semiconductor channel and a gate electrode separated by a dielectric from the channel[33, 34]. When biomolecules are introduced into the bio-FET, their corresponding interactions change carrier distributions of the channel resulting in a change of the electrical conductivity [35]. FETs are highly sensitive to their surroundings, however, they offer a low selectivity. In order to increase the selectivity of the FET biosensor, biomolecules called probes are immobilized on their surface through appropriate

linkers. Depending on the probe type, the FET biosensors are classified into four categories of aptamer, DNA, enzymatic, and immune FET biosensors (**Figure 1**).

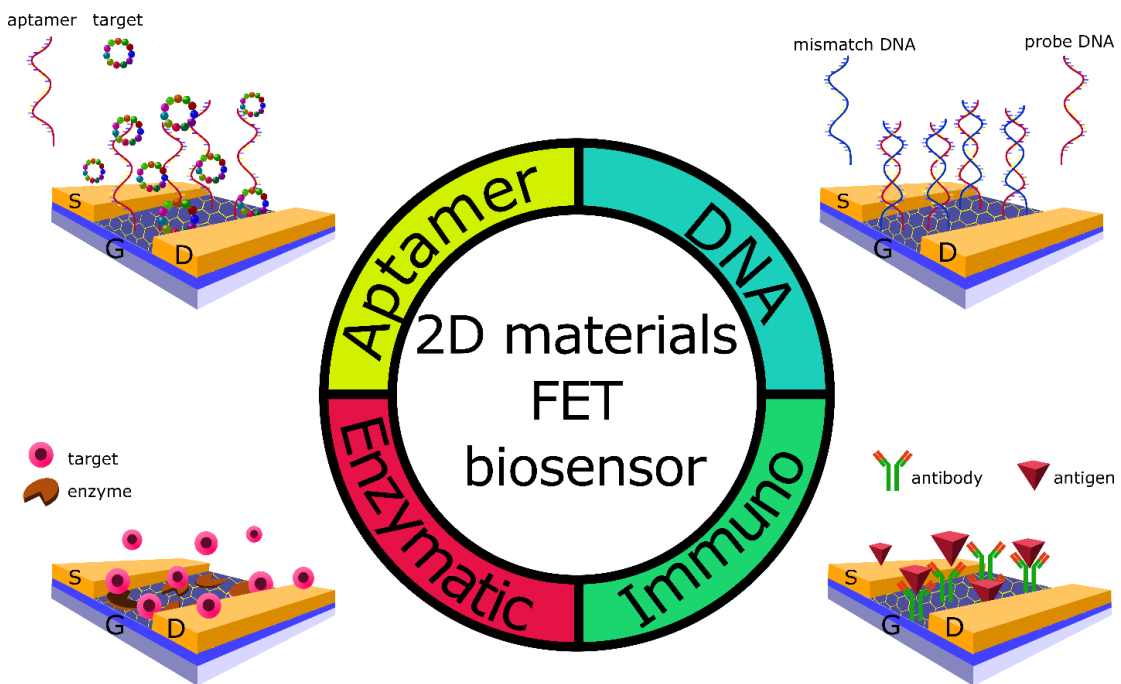


Figure 1. 2D based aptamer, DNA, immuno, and enzymatic FET biosensors.

To date, a variety of semiconductor materials have been used as a channel in the FET biosensors including metal oxides, carbon nanotubes, polymer-based compounds, inorganic materials, and various composites [35-39]. In 2004, a carbon monolayer known as graphene was discovered and has brought a great revolution in the field of material science [40]. Distinct properties of the one-atom-thick graphene attract increasing attention among research communities. The large surface area and high electrical conductivity of graphene promote it as a promising candidate for sensing applications [41, 42]. However, graphene is not alone and today, the 2D material family consists of numerous structures with unique properties [43-49]. Large detection surface area, remarkable carrier field-effect mobility, high sensitivity, acceptable biocompatibility, and easy surface functionalization of the 2D based FETs make them a superior candidate for biosensing applications [50-54].

This review focuses on 2D based bio-FETs and their related configurations. The basis of operation of the bio-FETs, target identifications, and signal detection are thoroughly discussed. Many of these biosensors perform detection in aqueous solutions where the Debye length, the isoelectric

point and pH play vital roles in affecting the final performance of the bio-FETs. Therefore, these essential concepts are introduced and their impact on the identification of biotargets is discussed. Two basic mechanisms of biotarget detection named doping and gating charge transfer are explained in this class of biosensors. Then, different 2D based bio-FETs are presented and their merits are accurately compared with each other. One of the biggest challenges facing these biosensors is the ability to detect targets in biomedical samples. Therefore, in the final part of this review, the clinical performance of the 2D based bio-FETs are discussed where promises a great development of the PoC devices.

1. 2D bio-FET configurations

Most 2D bio-FETs include three main parts: 1) Source/drain contacts 2) 2D channel composed of the sensitive biological material and 3) gate electrode (solution or back gates). Source/drain contacts can be metallic or even 2D conductive materials such as graphene. These electrodes are responsible for supplying electrical charge within the channel. The 2D material serves as a channel of the bio-FET and is responsible for the recognition of target biomolecules. For this purpose, the 2D layer is first functionalized with appropriate linkers in order to immobilize probes that are responsible for binding with the target biomolecules[34]. The detection mechanism can be based on direct charges transfer, induction of an electrostatic voltage, redox reactions, or any other interactions between biotargets and 2D layers that lead to a shift in the electrical conductivity of the FETs [55-58]. The third part of the bio-FETs, gate electrode can be a back- or a solution- gate called dry- or wet- states, respectively[59]. In dry-state operation (**Figure 2a**), an oxide layer acts as a dielectric, which is embedded beneath or above of the channel [59]. In wet-state operation (**Figure 2b**), a buffer solution acts as a dielectric and gate voltages are commonly applied through metallic electrodes such as Ag/AgCl, Ag, Pt wires, and so on [59-61].

The main detection mechanisms in 2D bio-FETs are based on two principles: doping effect[62-65] and electrostatic gating effect[66, 67]. In the doping effect, a direct charge transfer occurs between the probe-target duplex and 2D channel material (**Figure 2c**). As an example, in a pristine graphene-based FET (GFET), the minimum conductivity or called Dirac point (σ_{\min}) is generally observed at zero gate voltage ($V_g=0$). However, it usually involves a shift toward positive or negative voltages after being functionalized with linkers or being immobilized with probes. Regardless of this shift, as the probe-target binding occurs, this interaction may donate electrons (called n-doping) or accept electrons (called p-doping) [62-65]. The n-doping biotargets drive the

σ_{\min} to the negative gate voltages[62, 65], while the p-doping biotargets move the Dirac point to the positive gate voltages (**Figure 2d**)[63, 64]. In contrast, the gating effect appears due to accumulation of charges on the surface of the channel arising from probe-target binding which create a local external voltage drop across the channel[66, 67]. In the case of GFET, positively charged biotargets lead to a shift of σ_{\min} to the negative gate voltages, while the negatively charged biotargets result in a transfer of σ_{\min} to the positive gate voltages (**Figure 2e**) [66, 67]. In practice, both mechanisms may be involved in the biotarget sensing process that directly affect the drain current of the bio-FETs.

Among the various configurations of the 2D bio-FETs, electrolyte-gated FETs have attracted more attention thanks to their higher sensing performances compared with the dry-state cases [59]. They could be also integrated with a Polydimethylsiloxane (PDMS) microchannel or well to provide an effective target delivery on the surface of the channel[68]. Due to lower electrical resistances of buffer solution (in general, the resistance depends on ion concentrations), most of the applied gate voltage drops on a double layer formed in 2D/electrolyte interface known as an electrical double layer (EDL)[69-71]. The EDL induces a capacitance (called C_{dl}) that absorbs the opposite charges inside the channel in which the electrolyte acts as a dielectric [72]. Since the EDL thickness is about a few nanometers, the induced capacitance will be several orders of magnitude higher than the induced back-gate capacitance [59]. Therefore, the conductivity of the bio-FET in a wet state is more sensitive than in a dry state and can be modulated with small charge perturbations[59]. In addition to C_{dl} , the applied gate voltage is dropped across another capacitor known as quantum capacitance (C_Q)[73]. The C_{dl} value is calculated according to the equation, $C_{dl}=\epsilon_r\epsilon_0 A/\lambda_D$, where ϵ_r is the relative permittivity of the electrolyte, ϵ_0 is vacuum permittivity, A is the common area of 2D channel/electrolyte interface, and λ_D is the Debye length[73]. C_Q originates from changes in total charge to chemical potential (Fermi level, E_F) of 2D material and is defines as $C_Q=dQ/dE_F$ [74]. Both parts contribute to the total capacitance as follow[73, 74]:

$$\frac{1}{C_{tot}} = \frac{1}{C_{dl}} + \frac{1}{C_Q} \quad (1)$$

2D materials have a higher quantum capacitance compared to other materials[74]. Indeed, a small change in their density of state (DOS) results in a significant change in their Fermi level[74]. In general, C_{dl} is usually one order of magnitude larger than C_Q , which leads to a dominant contribution of C_Q in the total capacitance[75]. Therefore, any accumulation of biotargets on the

surface of the 2D channel leads to a considerable change in its Fermi level and subsequently changes the total capacitance. Hence, it results in the detection of the biotargets by modulation of the conductivity.

In solution-gated bio FETs, Debye length (λ_D) plays a key role in determining the limit of detection (LOD)[76]. The LOD refers to the lowest detectable amount of biotarget measured by the biosensor and expresses in terms of concentration (or amount). The Debye length is a distance where a net charge is screened to 1/e of its maximum value. The accumulation of buffer ions around the biomolecules is responsible for this screening. The λ_D is defined as[77]:

$$\lambda_D = \sqrt{\frac{\epsilon_r \epsilon_0 K_B T}{2 N_A e^2 I}} \quad (2)$$

Where $\epsilon_0 \epsilon_r$ is dielectric constant of electrolyte, $K_B T$ is thermal energy, N_A is Avogadro number, e is electron charge, and I is the ionic strength of solution. Accordingly, a solution with a higher ionic concentration has a shorter screening length while longer λ_D occurs at lower ionic concentrations[78].

A variety of buffer solutions such as phosphate-buffered saline (PBS), saline-sodium citrate (SSC), sodium fluoride (NaF), water, and Potassium chloride (KCl) are employed as an electrolyte in bio-FETs[79-82]. Among them, PBS is widely used because it is not only biocompatible but also has ionic concentrations similar to the human body. However, solutions with different ionic concentrations provide different Debye lengths [83]. Panel (f) to (h) of **Figure 2** demonstrate schematic illustrations of the detection process in three PBS solutions with different ionic concentrations. Accordingly, phosphate buffer concentrations of 0.01 M (1×PBS), 0.1 M (0.1×PBS), and 0.01 M (0.01×PBS) have λ_D of approximately 0.7, 2.4, and 7.4 nm, respectively[83]. As a result, a buffer solution with a longer λ_D detects biotargets more effectively since net charges screen over a longer distance[83]. It is noteworthy that the net charge of a specific biomolecule can be positive or negative depending on its isoelectric point (PI) value relative to the pH of the buffer solution[84, 85]. If PI is larger than the pH of the solution, H^+ ions protonate the carbohydrates and neutralize them, leaving only positive amine groups[85]. As a result, the biomolecule possesses a positive net charge in the corresponding solution.

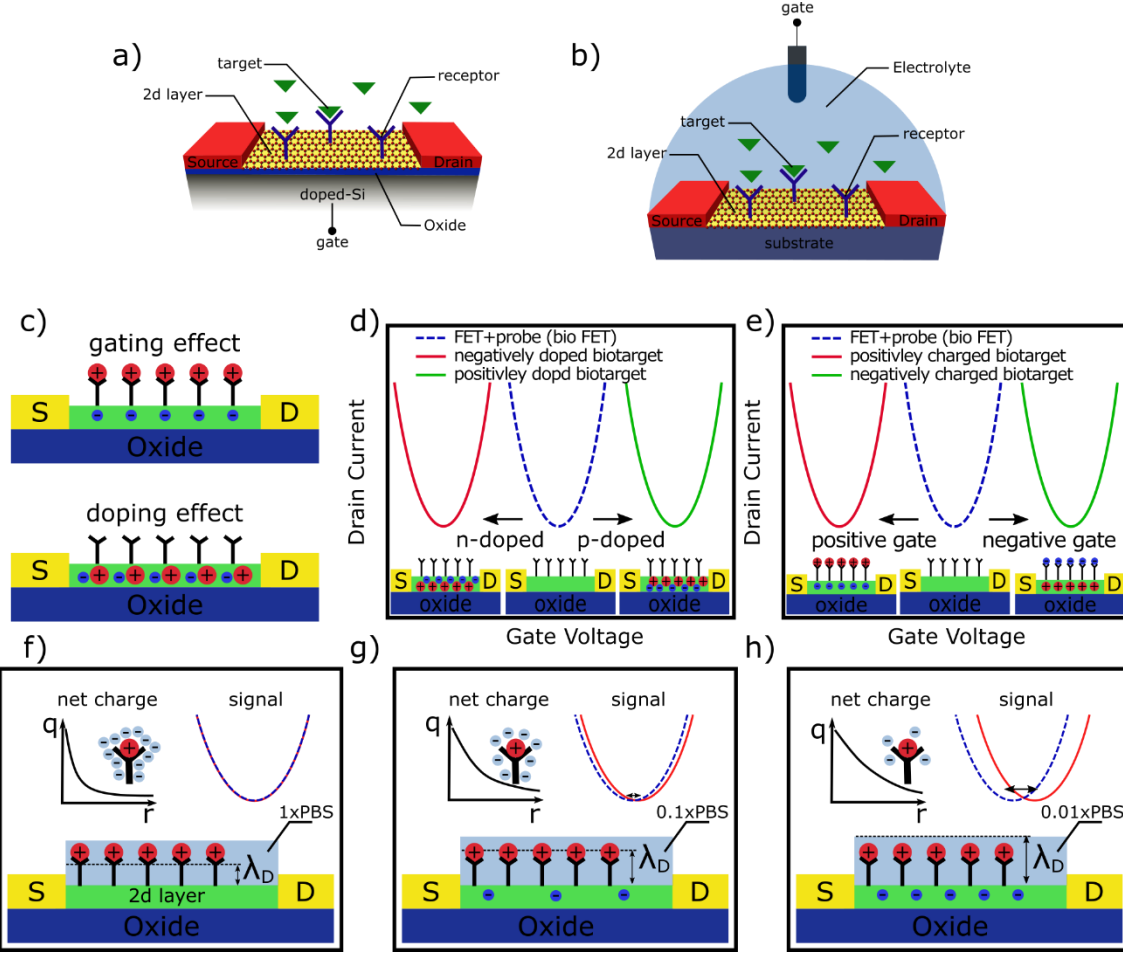


Figure 2. Schematic illustration of the 2D based **a)** back-gated and **b)** solution-gated bio-FET configurations. **c)** Doping and gating effects. Change of I_{ds} - V_g characteristics upon **d)** doping effect and **e)** gating effect. Solution-gated bio-FETs containing different PBS concentrations with corresponding Debye lengths. **f)** $1\times$ PBS. **g)** $0.1\times$ PBS. **h)** $0.01\times$ PBS.

1.1. 2D based FET aptasensors

Aptamer, a single-stranded DNA or RNA molecule, is artificially generated by an in vitro selection technique called systematic evolution of ligands by exponential enrichment (SELEX) method[86]. In this method, large randomized oligonucleotide sequences are synthesized and a specific aptamer is designed for the proposed biotargets via an iterative process in which aptamers binding to the specific biotargets are enriched. As a result, high-affinity aptamers with high specificity can be made using these complementary sequences[86]. Simple synthesis, low-cost production, thermal stability, and low immunological activity are some advantages of aptamers[86-88]. The discovery of aptamer brings new opportunities in the development of biosensors to detect various biotargets

with higher selectivity and sensitivity. FET aptasensors can detect various biomolecules by using specific aptamers, which are produced by the SELEX process and commercially are available.

With the increase in our knowledge of 2D materials, 2D bio-FETs have opened up new doors in introducing better-performing aptasensors. In this case, the specific aptamers are immobilized on the surface of the 2D channel through appropriate linkers. Linker molecules usually have pyrene functional groups that bind to the surface of the channel through π - π , van der Waals, and other interactions[89]. Metal nanoparticles such as AuNPs and PtNPs can also be used as linkers instead of organic molecules[64, 89]. In this case, the charge exchange between aptamer and nanoparticles is responsible for the binding. After immobilization of the aptamer probe, its specific target is introduced into the bio-FET. Depending on biotarget types, different interactions may occur between aptamer and target (such as electrostatic interactions, hydrogen bonding, and so on) where the corresponding binding results in a change of the drain current associating with detection of the biotarget[90].

Figure 3a shows a schematic illustration of a FET aptasensor configuration. In addition to organic linkers, metal nanoparticles such as AuNPs can also use as linkers (**Figure 3b**). The surface functionalization and aptamer immobilization can characterize with various analyses including atomic force microscopy (AFM), Raman spectroscopy, electrical characteristics, X-ray photoelectron spectroscopy (XPS), Energy-dispersive X-ray spectroscopy (EDS), and fluorescence microscopy methods[65, 67, 87, 88, 91]. In AFM analysis, thickness is measured after surface modifications[67, 88]. **Figure 3c** shows the measured thicknesses of single-layer graphene with and without functionalization after aptamer immobilizations[91]. It is observed that the thickness of the non-functionalized graphene remains at 0.3 nm while it increases to 2.5 nm in the case of functionalized graphene which refers to the successful immobilization of aptamers. In Raman analysis, coupling of pyrene groups of linkers with 2D material can affect both the position and intensity of oscillation modes of the 2D layer[65, 91, 92]. In the case of electrical measurements, linkers and aptamers change the conductivity or the transfer curve of the 2D FET due to their doping or gating effects[29, 65, 67, 92]. Moreover, they contain elements such as nitrogen and phosphorus, which XPS, EDS and fluorescence analyses can be employed to identify their presence [87, 91].

For applying gate voltages, different configurations have been introduced in 2D based FET aptasensors. For example, gate electrode can be placed planar next to the source and drain electrodes (**Figure 3d**)[93] or immersed in a buffer solution[63, 65, 67, 88, 91, 92]. In dry state bio-FETs, it is usually applied through a back-gated silicon[94].

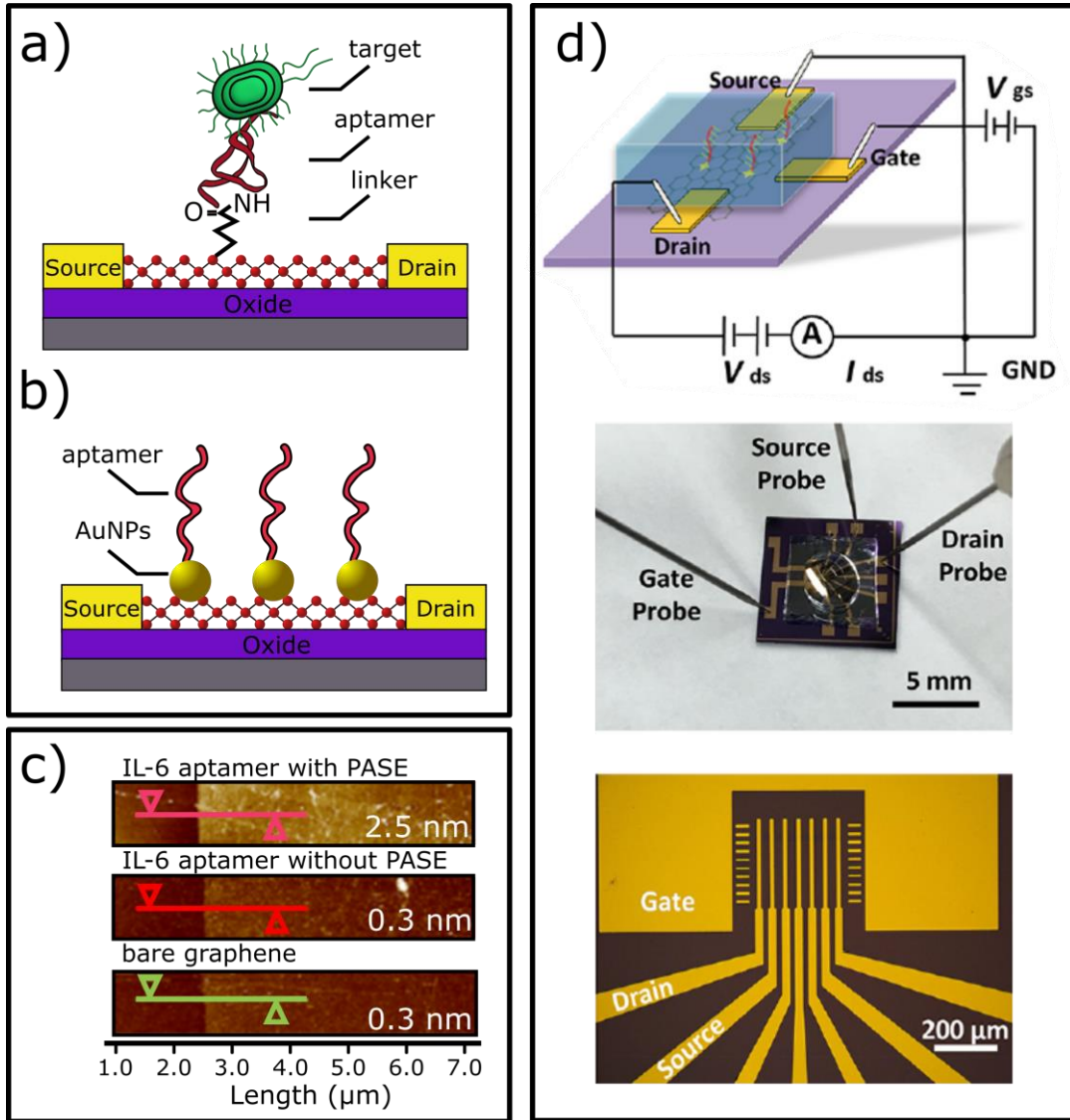


Figure 3. 2D-based FET aptasensors: **a)** Schematic configuration of a conventional aptamer bio-FET, and **b)** aptamer immobilizations via AuNPs linker. **c)** AFM measurements of aptamer immobilizations on graphene [91]. **d)** Schematic configuration of an aptamer bio-FET with a planar gate electrode (top), a photograph of the designed bio-FETs (center) and an optical image of the planar-patterned source, drain and gate electrodes (bottom) [93].

Among the large number of reported 2D-based FET aptasensors, special attention has been paid to graphene and Reduced graphene oxide (RGO), thanks to their available π - π interactions, large effective surface area, and environment-dependent electrical transports[29, 67, 87, 88, 93, 95]. Wu

et al. reported a graphene-based FET (GFET) capable of detecting *Escherichia coli* (E.coli) with a limit of detection (LOD) of 10^2 CFU/mL[67]. In this work, the specific aptamers are directly tagged with pyrene groups and immobilized on graphene. The binding of negatively charged E.coli bacteria to aptamer right-shifts the σ_{min} , like an electrostatic gate as shown in **Figure 4a**. Ghosh et al introduce a GFET to detect lysozyme in a range of 1 μ M to 100 nM[63]. Graphene surface is functionalized with 1-Pyrenebutyric acid N-hydroxysuccinimide ester (PASE) linkers through π - π interactions. Aptamers are then immobilized using amide bond formation with the –NHS of PASE[96]. The electron-rich nucleotide bases of aptamer lead to an n-doping effect while additional of the positively charged lysozyme imposes the p-doping effect and shifts the Dirac point to the positive gate voltage (**Figure 4b**). Hao et al. report a GFET for the detection of insulin in a dynamic range of 100 pM - 1 μ M with a LOD of 35 μ M[93]. Insulin acts as an n-dopant and denotes electrons to graphene. Farid et al. have observed a similar mechanism in GFET for detection of interferon-gamma (INF- γ) in which pyrene-modified aptamers are directly added to graphene [88]. Attachment of INF- γ to the modified graphene leads to an n-doping effect. In another report by Hao et al., a GFET is introduced to identify interleukin 6 (IL-6) in a range of 1 pM - 100 nM[91]. They employed an electric field between the Ag/AgCl gate electrode and the graphene surface to immobilize the PASE linker, which improved the LOD from 1.22 pM to 618 fM. Wang et al. utilized a GFET to detect tumor necrosis factor α (TNF- α) that plays an important role in cellular signaling[65]. In this report, the gate voltage is applied through a planar electrode and artificial tear is used as an electrolyte. TNF- α is detected through the n-doping effect with a LOD of about 2.75 pM. **Figure 4c** shows the response of the GFET to the various concentrations of TNF- α . Based on the electrostatic gating mechanism, Nekrasov et al., and Yang et al. use GFETs to detect ochratoxin A (OTA) and human epidermal growth factor receptor (HER2) biomolecules, respectively[92, 97]. In the latter, the positively charged HER2 screens the induced negative charge of the aptamer and acts as a positive electrostatic gate that decreases the drain current of the p-type GFET.

besides GFET, RGO bio-FETs (RFET) are widely used to detect various biomolecules. RGO is electrically charged due to its carboxyl groups and defects and can provide improved interaction with targets [87, 95]; [98]. An RFET with AuNPs linkers is used by We et al. to detect Hepatocellular Carcinoma-Derived Microvesicles (HEPG2-MVs) in a dynamic range of 500 pM-50 nM with a LOD of 4.8 pM[87]. MVs are bilayer lipids, released from cell membranes, and can

transport DNAs or proteins between cells[99]. HEP2-MVs play an intercellular communication role in HEP2 cancer cells and its identification is critical for cancer diagnosis[100]. The capture of HEP2-MVs by aptamer modified RFET results in the accumulation of negative charges on the RGO surface. In another work that is presented in **Figure 4d**, Kim et al. utilized RFETs to identify negatively charged protective antigens (PA) with a LOD of 12 aM [95].

Molybdenum disulfide (MoS_2) based FETs (MFET) are also employed to detect various biotargets based on aptamer probes. Chen et al. detects kanamycin (KAN) antibiotics in a dynamic range of 1 nM to 100 μM with a LOD of about 1.06 nM[94]. Aptamers are immobilized on MoS_2 surface via Au-S bonds and in order to increase sensitivity, short complementary strand DNAs (cDNA) are also attached to aptamers. The aptamer/CS complex folds together to form a shorter length of about 5.66 nm, which is less than the Debye length of the electrolyte ($\lambda_D \sim 5.88$ nm). By introduction of KAN molecules, CS is separated from aptamer and aptamer-KAN binding is formed via a non-covalent binding (**Figure 4e**). This process decreases the drain current of MFET since CS elimination results in less hole density in channel as can be seen in **Figure 4f**. In another work, Park et al. demonstrate that addition of different concentrations of cortisol is associated with a decrease in the drain current of the MFET[101].

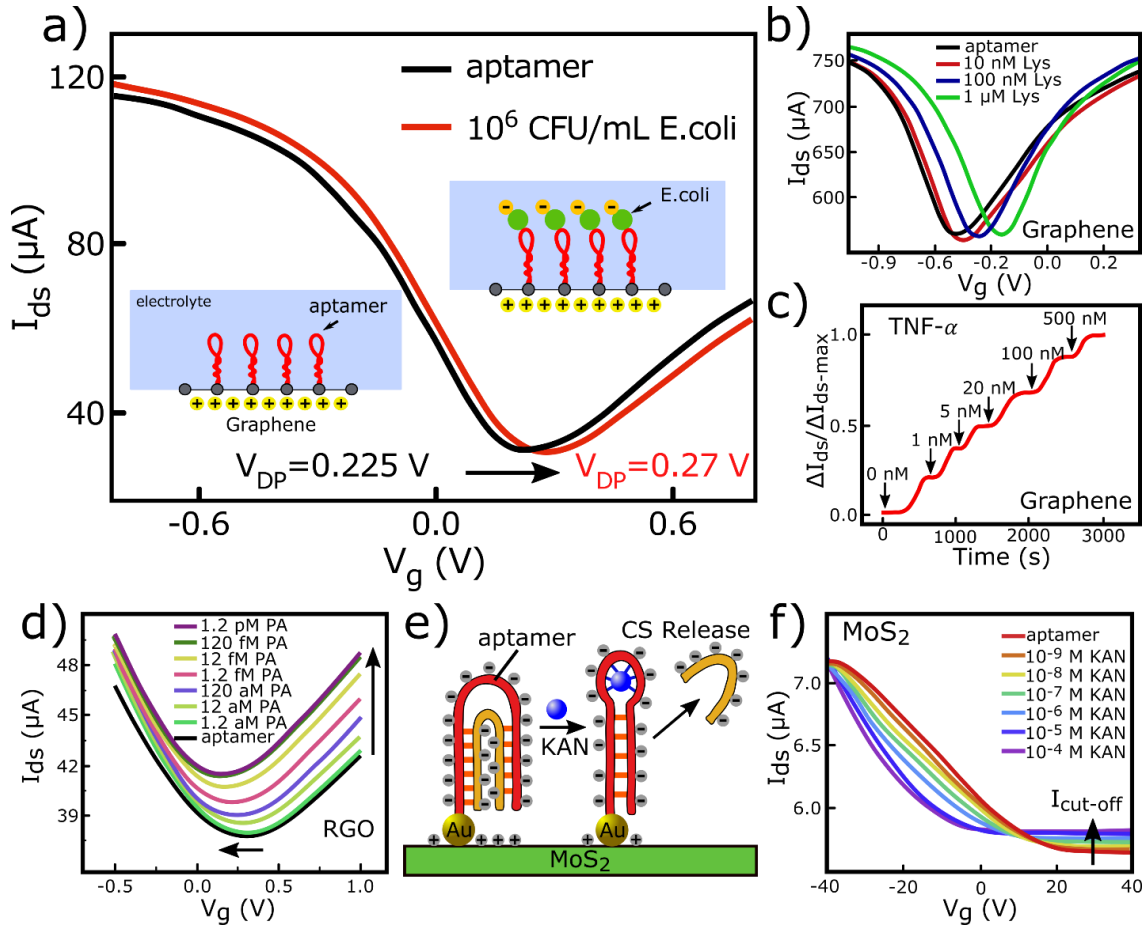


Figure 4. a) I_{dS} - V_g characteristics of GFET after immobilization of probe aptamer and in response to the E.coli targets[67], b) Transfer curve of the GFET under introduction of various concentration of Lys[63]. c) Time-resolved measurements of the GFET with different concentration of TNF- α [65]. d) I_{dS} - V_g dependency of RFET to different concentration of PAs[95]. e) schematic of the sensing mechanism in the MFET in response to KANs, and j) corresponding I_{dS} - V_g characteristics [94].

Table 1 shows a summary of different RGO, graphene, and MoS₂ based FET aptasensors. The table lists the biotarget type, dynamic range, linker, LOD, electrolyte, gate electrode material, and detection mechanism. According to the table, FET aptasensors are capable of detecting various biotargets in a wide dynamic range from aM to μ M with a high LOD.

Table 1. Performance summary of 2D based FET aptasensors in detection of various biotargets.

material	target	dynamic range	linker	gate electrode	electrolyte	LOD	sensing mechanism	ref
RGO	HepG2-Mvs	500 pM-50 nM	AuNPs	-	0.01×PBS	4.8 pM	n-doping	[87]
	Protective antigen	12 aM-120 fM	PASE	Pt wire	0.001×PBS	12 aM	n-doping	[95]
	HPV-16 E7	30-1000 nM	PCA	Ag/AgCl	10×PBS	1.75 nM	-	[102]

E.Coli	10 ² -10 ⁶ CFU/mL	Pyrene-tagged aptamer	Ag/AgCl	0.01×PBS	10 ² CFU/ml	gating	[67]	
Insulin	100 pM-1 μM	PASE	Planar Cr/Au	PBS	35 pM	n-doping	[93]	
IFN- γ	2 nM-100 μM	Pyrene-modified aptamer	Ag/AgCl	PBS	82.7 pM	n-doping	[88]	
IL-6 insulin	1 pM-50 nM	PASE	Ag/AgCl	1×PBS	618 fM 680 fM	doping	[91]	
TNF- α	0.03-500 nM	PASE	Planar Cr/Au	Artificial tear	2.75 pM	n-doping	[65]	
Graphene	OTA	10 pM-1 μM	PASE	Ag/AgCl	PBS	10 pM	gating	[92]
	Lysozyme	10 nM-1 μM	PASE	Needle	0.01×PBS	-	p-doping	[63]
	HER2	54 fM-1 nM	PASE	Ni/Au	1×PB	54 fM	gating	[97]
	Thr	1 pM-1 μM	PASE	Planar Au	0.01×PBS	2.6 pM	p-doping	[103]
	IL-6	100 pM- 100 nM	Pyrene-tagged aptamer	Planar Au	0.01×PBS	8 pM	n-doping	[104]
	CA1	0.3 pM- 3 nM	PASE	Pt wire	0.01×PBS	70 pM	gating	[105]
	IL-6	0-100 nM	PASE	back-gated Si	1×PBS	10.5 pM	-	[106]
	KAN	1 nM- 100 μM	AuNPs	back-gated Si	Dry state	1.06 nM	p-doping	[94]
MoS ₂	Cortisol	2.7 aM- 0.27 pM	APTES+GA	back-gated Si	Dry state	2.7 aM	-	[101]
	cTn1	10 fM-1 nM	APTES	-	1×PBS	10 fM	-	[107]

1.2. 2D based FET DNA biosensors

Cost-effective, rapid and highly sensitive DNA detection is of great importance in the diagnosis of genetic diseases, especially in the early detection of cancers[108]. Nucleic-acid diagnostics can play a valuable role in modern medicine by providing comprehensive information for medical experts. However, conventional DNA detection methods, including real-time PCR, molecular cloning, fluorescence assays and other methods are often faced with limitations such as low sensitivity, time-consuming and labor-intensive procedures[109-111]. Label-free FET biosensors, as a promising candidate is highly recommended thanks to their high selectivity, sensitivity, and versatility. Furthermore, their performance can be significantly improved by employing 2D materials as the active channel layers. In FET DNA biosensors, the single-strand DNAs called probe DNAs are immobilized via conjugation reactions between their amine groups with appropriate linkers[108]. In some reports, probe DNA is directly binded to the 2D surface without using linker molecules[62, 112, 113]. Target DNAs are then introduced into the bio-FET in order to be recognized. Due to the degree of genetic similarity, both probe and target DNAs are

hybridized through a complementary base pairing and form a single double-stranded molecule[114]. Therefore, the hybridization process results in the generation of an electrical signal in the bio-FET. In addition to DNA, RNA is also used as a probe. DNA backbones are made of deoxyribose, linked together via phosphates, while in PNA, backbones are made of repeating N-(2-aminoethyl)-glycine units linked together by peptide bonds[115].

Figure 5a shows a schematic illustration of the sensing procedure in a DNA bio-FET composed of linkers, probe DNA, target DNA and hybridization process. **Figure 5b** displays an AFM image of AuNPs as linkers on a GFET used for immobilizing of the probe DNAs[116]. The addition of linkers and probe DNAs is usually accompanied by an increase in the thickness of the 2D layer, which is one of the methods for characterizing the surface modification. According to **Figure 5c**, adding linkers and probe DNAs increase the thickness of graphene to ~2 and ~4nm, respectively[117]. As a case example, AuNPs linkers are used in an RFET by Cai et al. to immobilize PNA probes in order to detect cDNAs. The hybridization process is associated with n-doping effects in the bio-RFET while attachment of two other types of non-complementary and one-base mismatched DNAs do not show significant impacts on transfer curves of the FETs as shown in **Figure 5d**[118]. In another work, Yin et al. use PtNPs linkers to link probe DNAs on RFET through Pt-S covalent bonds[119]. The LOD of the bio-RFET is reported to be 2.4 nM in a dynamic range of 48 nM to 5 μ M.

In addition to RGO, there have been several reports of GFET DNA biosensors. Gao et al. used hairpin as a probe DNA to detect 21-mer in length target DNAs in a dynamic range of 1 fM to 100 pM[66]. A hairpin is a single-strand DNA in form of a double helix structure with an unpaired loop[120]. When target DNA is added, the hairpin is opened and a self-assembly reaction occurs between them in which DNA receives a negative charge and acts as an electrostatic gate (**Figure 5e**). Dong et al. suggest a GFET to detect 12-mer DNA with a LOD of 0.01 nM[62]. The DNA probe is directly immobilized on graphene through non-electrostatic stacking interactions. Zheng et al. immobilized 22-mer PNA probes on a GFET using PASE linkers to detect cDNAs in a dynamic range of 1 fM to 100 pM[121]. Among three different types of complementary, non-complementary, and one-base mismatched DNAs, a considerable drain current change occurs for cDNA thanks to its electron-rich nucleobases. Wang et al. utilized GA cross-linkers to immobilize 42-mer probe DNAs via a covalent bonding of $-\text{CH}=\text{O}$ to amino-group ($-\text{NH}_2$) of DNA[122]. Lin et al. immobilized 12-mer probe DNAs directly on graphene to recognize target DNAs in both dry

and wet ($1\times$ PBS) states[113]. They also employed Hall-effect measurements to investigate the evolution of carrier densities at different stages of surface modifications. **Figure 5f** shows that the hole density increases in both states for each modification stage, indicating p-doping effects. Xu et al. fabricated a GFET containing a PDMS block to detect 22-mer DNA targets (T20) based on the gating effect[123]. **Figure 5g** shows the photographic image of the introduced biosensors where the corresponding electrical measurements are presented in **Figure 5h**. The length of the probe DNA plays a direct role in determining the LOD of biosensors because it is somehow related to the Debye length. Ping et al. immobilized three different probe DNA lengths (22-mer, 40-mer, and 60-mer) on GFETs using PASE cross-linkers to detect the same target DNAs[117]. Their results show that as the length of cDNA increased, LOD improves from 100 pM to 1 fM.

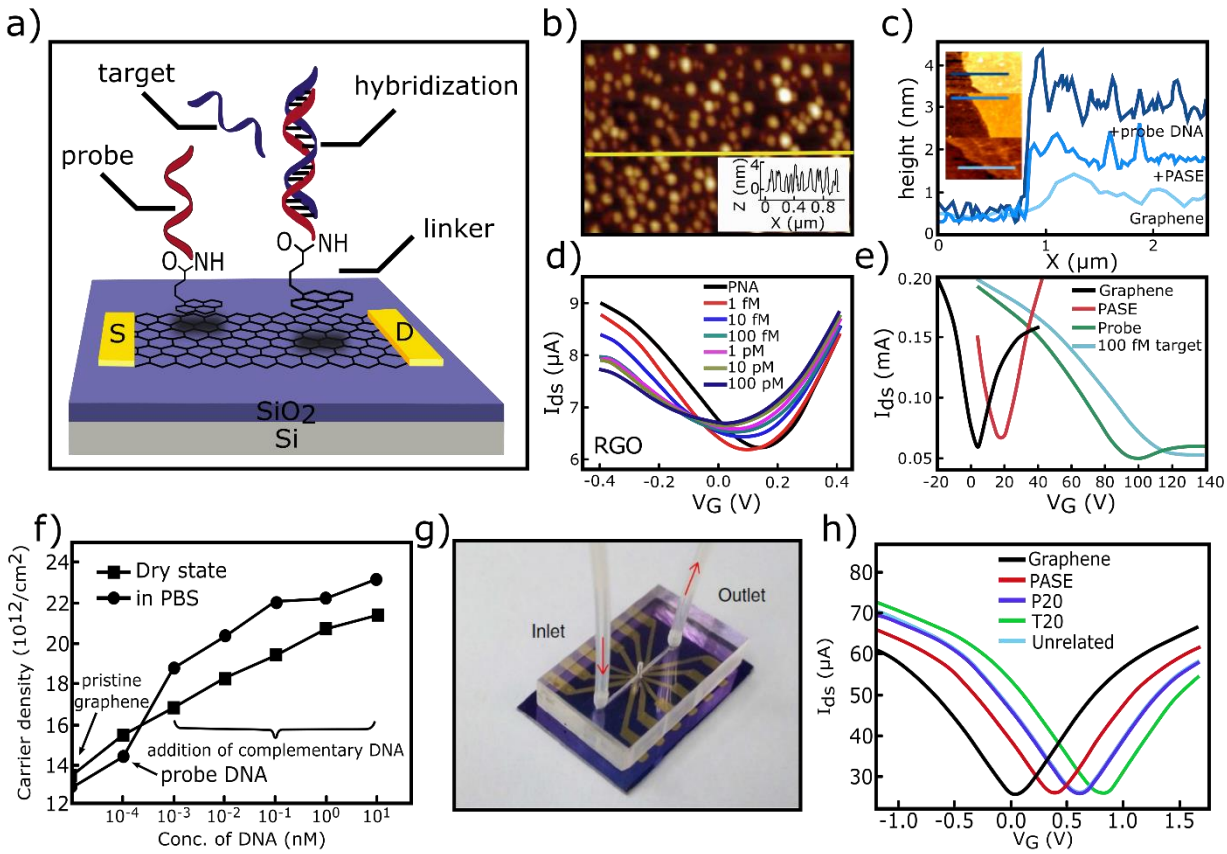


Figure 5. GFET DNA biosensors: **a)** Schematic illustration of a conventional DNA bio-FET. **b)** The AFM image of AuNPs on graphene as cross-linkers[116]. **c)** The measured thickness of graphene after modification with PASE linker, and probe DNA[117]. The I_{dS} - V_G characteristics of **d)** RFET with adding of various target DNAs[118], and **e)** GFET after modification with PASE linker, probe, and target DNAs in a dry state[66]. **f)** Hole density vs DNA concentrations in a GFET in both dry and wet ($1\times$ PBS) states at different stages of modifications[113]. **g)** Image of the DNA based bio-GFET with a PDMS block, and **h)** the corresponding I_{dS} - V_G characteristics[123].

Other 2D materials such as MoS₂ have been also employed in the 2D based DNA bio-FETs. **Figure 6a** shows a schematic of a bio-MFET introduced by Liu et al[124]. The photograph of the MFET is presented in **Figure 6b**. The surface modifications with AuNPs, probe DNAs, and target DNAs are controlled by Raman analysis as shown in **Figure 6c**. After the attachment of probe DNAs, the A_{1g} peak shifts blue due to its contribution as a p-dopant. The same trend is also observed after DNA hybridizations[124]. Therefore, according to **Figure 6d**, the decrease in drain current (I_{ds}) originates from the decrease in the electron density within the MFET channel during DNA hybridizations. Based on the gating mechanism, Lee et al. detect 18-mer probe DNAs as follows: phosphate backbones of the probe DNAs are negatively charged where their accumulation on MoS₂ reduces the electrons density within the MFET channel. Hybridizations result in a reduction of the binding interactions of the DNAs with the 2D layer which causes the hybridized DNAs to leave the MoS₂ surface. This phenomenon ends with increases of I_{ds} current in the MFET (**Figure 6e**)[112]. Mie et al. immobilize phosphorodiamidate Morpholino oligomer (PMO) as a probe on few-layered MoS₂ via PASE cross-linkers[125]. PMO has a similar structure to DNA, except that instead of deoxyribose rings, it has morpholino rings linked together by phosphorodiamidate bonds[126]. In their report, MFET exhibits a p-type behavior and drain current is reduced by the addition of the cDNA. **Figure 6f** shows the current response of the bio-MFET to different targets, with the highest sensitivity to cDNA.

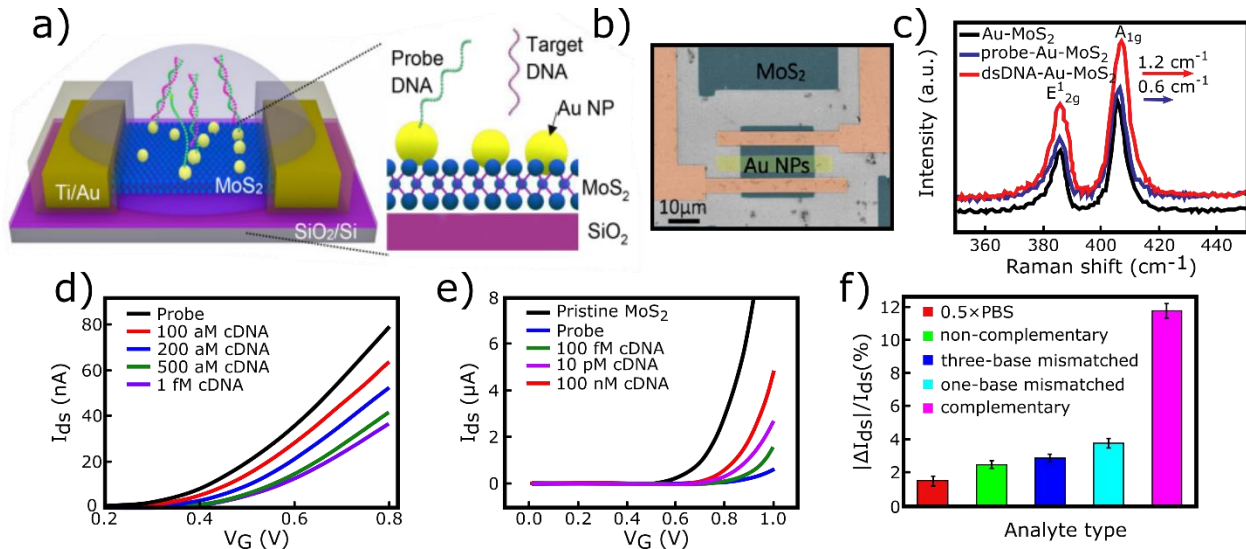


Figure 6. Beyond graphene DNA bio-FETs. **a)** Schematic illustration of a MoS₂ biosensor, **b)** image of its channel with AuNPs linkers, **c)** Raman analysis of modification states, and **d)** the corresponding I_{ds}-V_G curves in response to various concentrations of target DNAs[124]. **e)** Transfer curves of a bio-MFET after immobilizing of probe and target DNAs[112]. **f)** Response of bio-MFET to different target DNAs[125].

A summary of the performance of the DNA bio-FETs based on the various 2D materials and related testing parameters are presented in **Table 2**. These biosensors are able to detect different lengths of target DNAs from 15-mer to more than 60-mer with a wide dynamic range.

Table 2. Performance summary of 2D based-FET DNA biosensors in the detection of various target DNAs.

material	Target DNA	dynamic range	linker	gate electrode	electrolyte	LOD	sensing mechanism	ref
RGO	22-mer	1 fM-100 pM	AuNPs	Ag wire	1×PBS	10 fM	n-doping	[118]
	22-mer	10 fM-1 nM	PASE	Ag wire	1×PBS	100 fM	n-doping	[108]
	22-mer	48 nM-5 μ M	PtNPs	Pt wire	PBS	2.4 nM	n-doping	[119]
Graphene	21-mer	1 fM-100 pM	PASE	back-gated Si	Dry state	5 fM	gating	[66]
	12-mer	0.1-10 nM	Linker free	Ag wire	PBS	0.01 nM	n-doping	[62]
	22-mer	1 fM-100 pM	PASE	Ag wire	0.01×PBS	10 fM	n-doping	[121]
	42-mer	1 fM-10 μ M	GA	Pt wire	PBS	10 fM	-	[122]
	12-mer	1 pM-10 nM	Linker free	Ag wire	1×PBS	1 pM	n-doping	[113]
	22-mer	0.25-10 nM	PASE	Pt wire	0.01×PBS	10 pM	gating	[123]
	15-mer	100 fM-1 nM	PASE	Ag/AgCl	0.01×PBS	100 fM	gating	[127]
	22-mer	100 pM- 100 nM	PASE	Ag/AgCl	0.1×PBS	0.1 nM	gating	[128]
	22-mer					100 pM		
	40-mer	1 fM-100 μ M	PASE	back-gated Si	Dry state	100 fM	gating	[117]
Graphene/MoS ₂	60-mer					1 fM		
	24-mer	0.1- 10^4 nM	AuNPs	back-gated Si	Dry state	1 nM	gating	[116]
	15-mer	100 aM-1 pM	PASE	Ag/AgCl	0.1×PBS	100 aM	gating	[129]
	22-mer	600 zM- 60 nM	PASE	Ag/AgCl	0.1×PBS	600 zM	gating	[130]
MoS ₂	15-mer	10 aM- 100 pM	PASE	Ag/AgCl	1×PBS	10 aM	gating	[131]
MoS ₂	30-mer	100 aM-1 fM	AuNPs	Ag wire	0. 1×PBS	100 aM	p-doping	[124]
	18-mer	10 fM-100 nM	Linker free	Ag/AgCl	0. 1×PBS	10 fM	gating	[112]
	22-mer	10 fM-1 nM	PASE	Ag wire	PBS	6 fM	-	[125]

1.3. 2D based FET immunosensors

In FET immunosensors, antibodies (Abs) are immobilized as probes on the FET channel by appropriate linkers to detect antigens or biomolecules containing antigens[64, 132-135]. Immunoglobulin, or antibody, is a Y-shaped protein that contains different chains of peptides produced by immune system (plasma) cells[136]. Antibodies can recognize biomolecules called antigens (Ags) or even organic chemicals. Ag is composed of proteins or peptides and can match with binding sites of the specific Ab to form an antibody-antigen complex[137]. When an Ag (target biomolecule) introduces into a bio-FET, its binding to Ab generates a detectable electrical signal and subsequently changes the drain current. This feature is highly efficient in identifying

many cancer biomarkers, bacteria, viruses, and proteins[138-144]. In addition, the use of 2D materials as a channel in the bio-FETs dramatically increases their performance efficiency.

Figure 7a shows a schematic illustration of a conventional GFET immunosensor with source/drain contacts, graphene as a channel, linkers, probes (Ab), and targets (Ag). Various linkers are employed in the GFET immunosensors such as PASE, metal nanoparticles, 1-pyrenemethylammonium chloride (PyMA), and EDC/NHS[132-134, 142, 143]. **Figure 7b** demonstrates an SEM image of an RFET decorated with PtNPs linkers to detect brain natriuretic peptide (BNP), a useful hormone in diagnosing heart failure, with a LOD of 100 fM[64]. Anti-BNP (probe) is negatively charged at pH of 7.4 since its isoelectric point (PI) is in the range of 6.6 to 7.2. Its immobilization results in an increase of electron density within the channel of RFET. In contrast, BNP Ag (target) is positively charged and its addition acts as a p-dopant as shown in **Figure 7c**. Yu et al. fixed CD63 Abs on a PASE functionalized RGO to detect exosome which contains CD63 Ags on its surface[135]. Exosome has a negative charge and its introduction results in an n-doping of the bio-RFET. **Figure 7d** compares the change of Dirac voltage in response to four different types of biotargets: carcinoembryonic antigen (CEA), alpha-fetoprotein (AFP), bovine serum albumin (BSA) and exosome, where the highest selectivity is for the latest. In another report, Kim et al. used RGO to detect prostate specific antigen-alpha-1-antichymot (PSA-ACT) in two different buffer solutions with pH of 7.4 and 6.2 where PSA-ACT complex is negatively and positively charged at these pH, respectively[132]. According to **Figure 7e**, with the addition of PSA-ACT, Dirac voltage shifts to negative (at pH 7.4) and positive (at pH 6.2) gate voltages. Thakur et al. sensed E.coli cells based on the gating effect in a functionalized RGO[134]. A nanometer-thick Al_2O_3 layer is placed between AuNPs linkers and the RGO channel. Adding the negatively charged E.coli cells to positively charged Abs neutralizes Ab net charges and reduces the induced positive gate potential over the channel.

Along with RGO, several reports have been published based on the GFET immunosensors. Seo et al. employed graphene to detect respiratory syndrome coronavirus 2 (SAR-CoV-2) with a detection limit of 0.01 fM to 0.1 pM in PBS buffer and clinical solutions, respectively[144]. **Figure 7f** shows a schematic of the introduced immunosensor. The real-time response of the bio-GFET to different concentrations of SAR-CoV-2 is displayed in **Figure 7g**. Mao et al. functionalized vertically-oriented graphene with AuNPs to detect the most common Ab in human blood called immunoglobulin G (IgG)[133]. Based on it, the addition of IgG is associated with a decrease in I_{ds}

current of the bio-GFET. Jung et al. utilized CVD-grown graphene to identify carbohydrate Ags 19-9 (CA 19-9), a marker of pancreatic cancer, at two different pH of 5.8 and 9.4 in 10 μ M PBS buffer solutions[140]. CA 19-9 behaves as p-dopant and n-dopant at pH values of 5.8 and 9.4, respectively. Haslam et al. used a GFET to detect human chorionic gonadotropin (hCG) protein in dry state conditions with a LOD of 2 fM [139]. Increased concentration of hCG hormone in the body can be a sign of testicular cancer, prostate cancer, pancreatic cancer or even pregnancy[145]. Kwong et al. identified exosomes in a dynamic range of 1 nM - 0.1 μ M with a LOD of 1 nM on the surface of a functionalized graphene[141]. Exosomes contain a great deal of genetic information about cells by which they are secreted, and its identification is helpful in the early detection of cancers[146]. In their work, the anti-CD63 Abs immobilized on graphene with PASE linkers and different concentrations of the exosomes (in PBS solution) were directed to the surface of the bio-FET channel through a PDMS channel. Attachment of exosomes is associated with the electrostatic gating effect. Rajesh et al. immobilized anti-HER3 ScFv on PtNPs decorated graphene to detect HER3 Ags with a detection limit of 1.6 fM[142]. HERs involve information about some tumors such as breast cancer and gastric cancer[142]. Thiol-containing single-chain variable fragment (ScFv) Abs are used as probes, which consists of two light (V_L) and heavy (V_H) chains that are connected by a peptide linker. 0.1% Tween 20 is also used to block non-specific sites (**Figure 7h**). The electrostatic gating effect originated from the Ag-Ab binding is responsible for the detection of the Ags (**Figure 7i**). Mechanically exfoliated graphenes were employed by Roberts et al. to detect Japanese encephalitis virus (JEV) and avian influenza virus (AIV)[143]. The detection mechanism is described by the reduction of the current through the gating effect. **Figure 7j** shows the response of a bio-GFET fabricated by Gao et al. to identify *Borrelia burgdorferi* (*B. burgdorferi*) bacteria, which causes Lyme disease[138]. Two types of anti-IgG and GroEs scFv Abs are used as probes. The LOD of the biosensor is measured to be about 1.3 nM in presence of the anti-IgG probe, which improves to 0.3 pM with GroEs scFv Probe. This difference stems from the fact that scFv Abs (with a length of ~2.2 nm) capture Ags closer to the surface of graphene compared with the anti-IgG (with a length of ~6.9 nm).

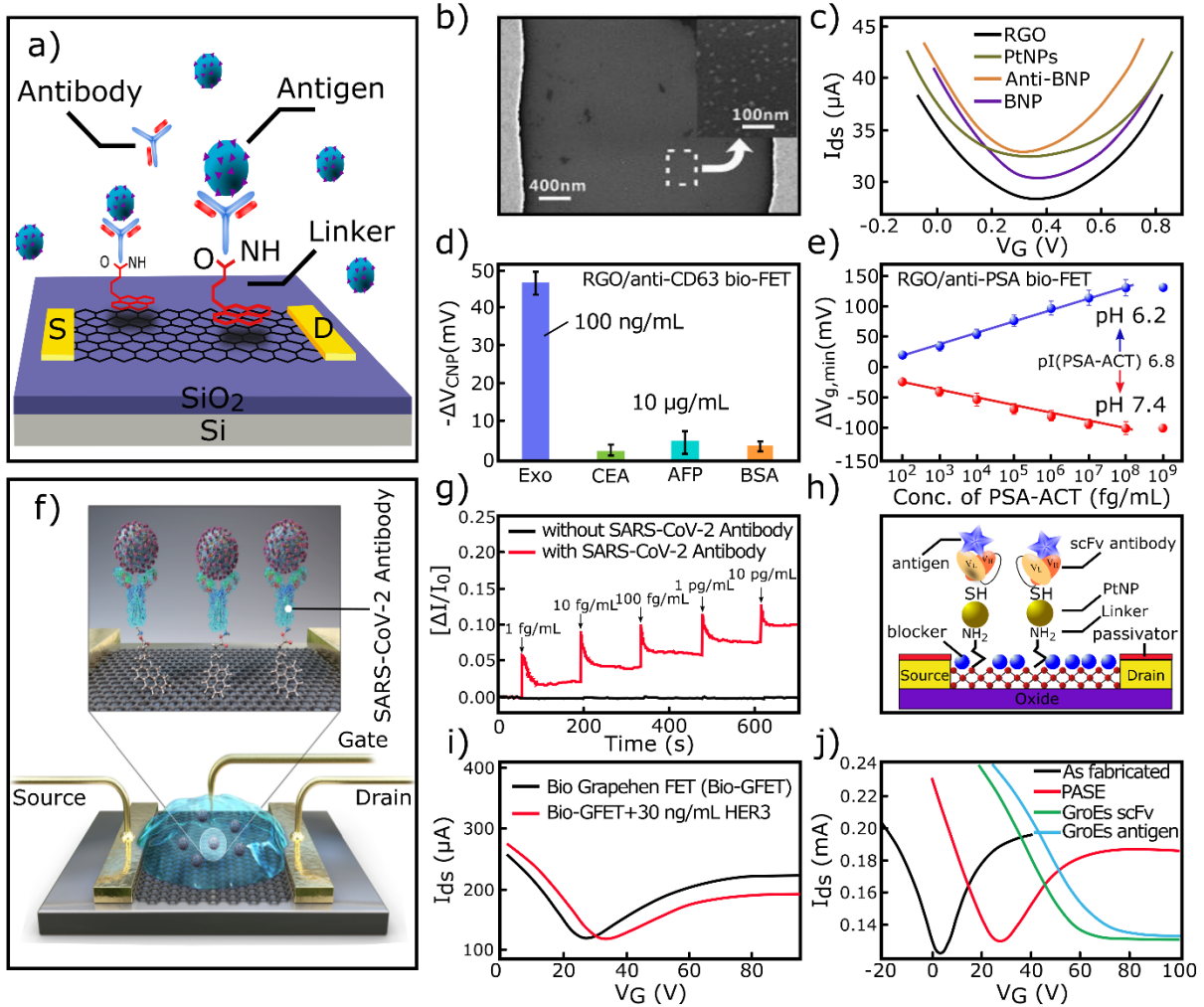


Figure 7. GFET immunosensors. **a)** Schematic illustration of a conventional bio-GFET. **b)** SEM image of an RFET decorated with PtNPs linkers and **c)** its I_{ds} - V_g characteristics for each stage of modifications[64]. **d)** Change of the Dirac voltage in response to four different biotargets in RGO[135]. **e)** Variation of $\Delta V_{g,min}$ with PSA concentrations in RGO for two testing pH buffer solutions[132]. **f)** Schematic illustration of a bio-GFET for detection of SARS-CoV-2 virus and **g)** real-time sensing in response to SARS-CoV-2 Ags[144]. **h)** Schematic illustration of a bio-GFET with all its components and **i)** corresponding I_{ds} - V_g curves in response to 30 ng/mL (0.16 nM) HER3 Ags[142]. **j)** Transfer curve of the graphene after modification with linkers, GroEs scFv antibody and attachment of GroEs antigen[138].

In addition to GFETs, FET immunosensors based on other 2D materials such as TMDs (MoS_2 , WSe_2), back phosphorous (BP), and indium oxide (In_2O_3) have been introduced up to date. These 2D materials are generally functionalized by APTES and GA, or in some cases with metal nanoparticles (NPs) and EDC/NHS method, similar to GFETs[147-150]. A schematic illustration of TMD-based FET immunosensors can be seen in **Figure 8a**. Nam et al. embedded MoS_2 and WSe_2 layers separately on FET channels to detect $\text{TNF-}\alpha$ in a 60 fM-6 pM dynamic range (**Figure 8b,c**)[149]. Adding $\text{TNF-}\alpha$ to the functionalized FETs reduces the electron densities in both layers referring to p-doping effects (**Figure 8d**). Similarly, Chen et al. sensed $\text{TNF-}\alpha$ biomolecules with

a LOD of 60 fM based on a MoS₂ bio-FET[151]. Ryu et al. functionalized MoS₂ FET with APTES and Ga linkers to immobilize anti-IL-1 β Abs [150]. In a four-step process called IFDM cycle (Incubation-Flushing-Drying-Measurement), IL-1 β is detected in a dynamic range of 1 to 500 fM with a LOD of 1 fM through an electrostatic gate effect. In another report by Park et al., Prostate-Specific Antigen (PSA) biotargets were identified by mechanically exfoliated MoS₂ FET with a LOD of 3 fM[152]. **Figure 8e** shows the detection process including surface functionalization with APTES and GA, Anti-PSA immobilization, non-specific sites blocking with casein, and attachment of PSA antigens. Both anti-PSA Abs and PSA Ags are positively charged, and their accumulations on MoS₂ induce electrostatic attractions (**Figure 8f**). In another work, Wang et al. applied a microfluidic channel PDMS block to a MoS₂ FET to detect PSA Ags[153]. The photograph of the fabricated biosensor can be seen in **Figure 8h**. The I_{ds-t} characteristics of the biosensor in response to three different concentrations of PSA are presented in **Figure 8i**. Dalila et al. introduced an MFET immunosensor that detected C-reactive protein (C-RP) Ags with a LOD of 0.06 fM[147]. **Figure 8g** shows the transfer curve of the biosensor in response to different concentrations of the biotargets. The positively charged C-RP Ags increase the density of electrons inside the channel leading to an increase of the drain current. Few layers of black-phosphorous (BP)-bio FET is introduced by Chen et al. to identify IgG[154]. In order to avoid surface passivation, the layer is covered by Al₂O₃ film. IgG proteins have a negative surface charge and their binding with Abs induce a negative gate voltage on the p-type BP-FET, which leads to an increase in current. **Figure 8j** shows the sensitivity versus target concentrations of the specific probe+IgG Ag, without probe+IgG Ag, and probe+avidin Ag the BP-FET. Accordingly, the highest selectivity is measured for IgG Ags.

Liu et al. used an In₂O₃ nanoribbon to identify three different biotargets of cardiac troponin I (cTnI), creatine kinase (CK-MB), and B-type natriuretic peptide (BNP), which are commonly associated with heart attack and heart failure[148]. Detection mechanism is reported based on a pH-dependent conductivity called the enzyme-linked immunosorbent assay (ELISA)[155]. This method relies on protonation/deprotonation of OH groups near the FET surface that results in local changes of the gate voltage across the channel. In this report, specific Abs are fixed through EDC/NHS linkers and bind with target Ags. The secondary Abs, which are also specific to the target Ags, bind to the Ags followed by coupling with streptavidins. The other end of the secondary Ab contains biotin where is linked to streptavidin. The biotin-streptavidin complex is one of the

preferred arrangements for conjugation with biomolecules[156]. The schematic of the ELISA method is illustrated in **Figure 8k**. Finally, addition of urease increases the pH of solution according to the following reaction:



Accordingly, the protonation of the hydroxyl groups on the surface increases the negatively surface charges and decreases current. The amplification of the detection signal and detection beyond the Debye length limit are advantages of the ELISA method. **Figure 8i** shows the real-time response of the biosensor for three different cTnI concentrations which adding 10 mM urea to the buffer solution results in a reduction of the drain current.

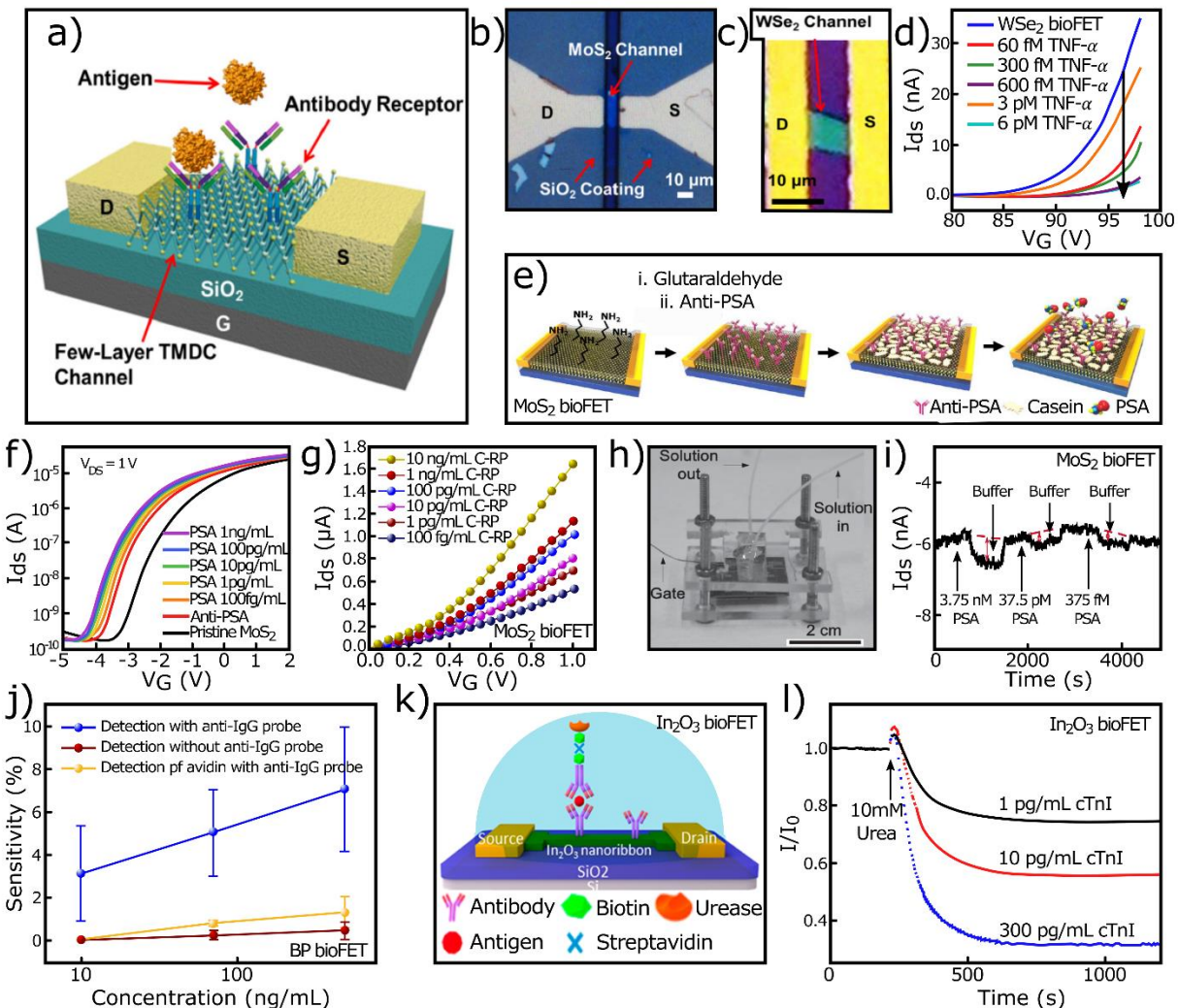


Figure 8. Beyond GFET immunosensors. **a)** Schematic illustration of a TMD based bio-FET[149]. **b)** image of MoS₂ channel, and **c)** image of WSe₂ channel, and **d)** I_{ds}-V_g characteristics of WSe₂ bio-FET in response to TNF- α Ags[149]. **e)** Schematic illustration of fabrication stages of a MoS₂ bio-FET, and **f)** its I_{ds}-V_g curves with addition of PSA Ags[152]. **g)** Transfer curve of a MoS₂ bio-FET in response to various concentration of C-RP biotargets[147]. **h)** Image of the

MoS₂ bio-FET with PDMS microfluidic block, and **i**) real time sensing to different concentrations of PSA Ags[153]. **j**) Sensitivity versus target concentration in a black phosphorous bio-FET[154]. **k**) Schematic illustration of ELISA detection method in an In₂O₃ bio-FET, and **l**) real time detection of cTnI Ags with different concentrations [148].

Table 3 shows a summary of 2D-based FET immunosensors, with corresponding parameters including types of biotargets, linkers, testing conditions, LOD, and the detection mechanism. FET Immunosensors can detect a variety of biomolecules with considerable sensitivity and LOD.

Table 3. Performance summary of 2D based FET immunosensors in detection of various Ag targets.

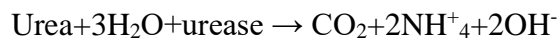
material	Target antigen	dynamic range	linker	gate electrode	electrolyte	pH	LOD	sensing mechanism	ref
Doped GO RGO	BNP exosome	10 aM- 1 μ M 1 fM- 0.1 pM	Linker-free PASE	back-gated Si back-gated Si	Buffer PBS	7.0 7.4	10 aM 1 fM	gating n-doping	[157] [135]
	PSA-ACT	1.1 fM- 0.01 μ M	PASE	pt wire	0.0001×PBS	7.4 6.2	1.1 fM	n-doping p-doping	[132]
	E. coli	10^3 - 10^5 CFU/mL	AuNPs+EDC/NHS	back-gated Si	Dry state	-	10^3 CFU/mL	gating	[134]
	BNP	100 fM-1 nM	PtNPs+EDC/NHS	Ag wire	0.001×PBS	7.4	100 fM	p-doping	[64]
	IgG	13 pM-0.1 nM	AuNPs	back-gated Si	Dry state	-	13 pM	-	[133]
Graphene	CA 19-9	0.01-1000 unit/mL	PASE	Ag/AgCl	0.001×PBS	9.4 5.8	0.01 unit/mL	n-doping p-doping	[140]
	HER3	1.6 fM- 1.6 mM	PyMA+PtNPs	back-gated Si	0.1×PBS	7.3	1.6 fM	gating	[142]
	hCG	2 fM- 20 pM	PASE	back-gated Si	Dry state	-	2 fM	-	[139]
	exosome	1 nM- 0.1 μ M	PASE	back-gated Si	PBS	7.0	1 nM	gating	[141]
	JEV AIV	1 fM-1 μ M	EDC/NHS	back-gated Si	5×PBS (50 mM)	7.4	1 fM 10 fM	gating	[143]
MoS ₂ WSe ₂	B. burgdorferi	0.3 pM- 3 nM	PASE	back-gated Si	Dry state	-	0.3 pM	gating	[138]
	SARS-CoV-2	0.01 fM- 0.1 pM	PASE	-	PBS	7.4	0.01 fM	-	[144]
	Clusterin	10 fM- 1.6 pM	Pyr-NHS	back-gated Si	Dry state	-	5 fM	-	[158]
	TNF- α	60 fM-6 pM	APTES+GA	back-gated Si	Dry state	-	60 fM	p-doping	[149]
	SARS-CoV-2	0.3 fM-0.1 nM	EDC/NHS	back-gated Si	0.01×PBS	-	0.3 fM	gating	[159]
MoS ₂	PSA	0.3 fM- 0.03 nM	APTES	back-gated Si	Dry state	-	0.3 fM	gating	[160]
	PSA	375 fM-3.75 nM	APTES+GA	Ag/AgCl	0.01×PBS	6.68	375 fM	gating	[153]
	PSA	3 fM- 30 pM	APTES+GA	back-gated Si	Dry state	-	3 fM	gating	[152]
	C-RP	0.8 fM- 8 pM	AuNPs	back-gated Si	PBS	7.4	0.06 fM	gating	[147]
	TNF- α	60 pM-60 fM	APTES+GA	back-gated Si	Dry state	-	60 fM	-	[151]
BP	ConA	1 mM- 100 nM	AuNPs	back-gated Si	Dry state	-	105 nM	gating	[161]
	IL-1 β	1-500 fM	APTES+GA	back-gated Si	Dry state	-	1 fM	gating	[150]
	IgG	60 pM- 3 nM	AuNPs+GA	back-gated Si	0.01×PBS	-	60 pM	gating	[154]
In ₂ O ₃	cTnI	40 fM- 12 pM					40 fM		
	CK-MB	1 fM- 0.03 nM	EDC/NHS	Ag/AgCl	0.01×PBS	-	1 fM	gating	[148]
	BNP	3.3- 30 pM					3.3 pM		

1.4. 2D based FET enzymatic biosensor

The enzymatic reaction is responsible for generating a detectable electrical signal between probe enzyme and target biomolecules[162]. Enzymes are proteins that usually act as catalytic molecules

where their product of reaction affects the conductivity of the bio-FETs[81, 163, 164]. Similar to other FET biosensors, enzymes are immobilized on the surface of a 2D channel as probes through appropriate linkers.

Figure 9a shows a schematic of a GFET enzymatic biosensor[165]. **Figure 9b** demonstrates a GFET enzymatic biosensor introduced by Thanh et al to detect 1-naphthyl-N-methyl carbamate (carbaryl)[82]. Carbaryl is a chemical used to control insects in agricultural products, and excessive accumulation of it in food or water can lead to human poisoning[82]. To recognize carbaryl, first the urease enzymes are immobilized on the surface of graphene, and a mixture of urea/water is added to the biosensor to initiate the following reaction:



In the presence of urea and enzymes, NH_4^+ ions are produced by the hydrolysis of urea, leading to n-doping effects. This hydrolysis process is restricted by the introduction of carbaryl and results in less accumulation of NH_4^+ ions on graphene and right-shifts the Dirac point. Kwak et al. employed CVD-grown graphene to detect glucose in a range of 3.1-10.9 mM with a detection limit of 3.3 mM[165]. Glucose oxidase (GOx) is immobilized on the surface of graphene as a probe via PASE linkers. Glucose is catalyzed based on the enzymatic reaction by GOx, in which its reaction products are gluconic acid and H_2O_2 . The increase of glucose concentration leads to more production of H_2O_2 , which results in the n-doping effect. **Figure 9c** shows the I_{ds} - V_g characteristic of the bio-FET in response to different concentrations of glucose[165]. The corresponding schematic of this biosensor is also presented in **Figure 9a**. In another work, CVD-grown graphene was reported by Zhang et al. to detect glucose with a detection limit of 0.5 μM in a dynamic range of 0.5 μM -1 mM[166]. They used PtNPs as linkers to fix the GOx. Similarly, the glucose detection process is associated with the release of H_2O_2 and an increase in the drain current.

In addition to graphene, RGO has also been used as FETs in enzymatic biosensors. Park et al. used 4-(4,6-dimethoxy-1,3,5-triazine-2-yl)-4-methyl-morpholinium chloride (DMT-MM) linkers to immobilize GOx on RGO to detect glucose with a detection limit of 1 nM[164]. Piccinini et al. functionalized RGO with sodium 1-pyrenesulfonate (SPS) linkers followed by assemble of urease-polyethyleneimine (PEI) layers as probes to detect urea[81]. This enzyme accelerates the hydrolysis process of urea to produce NH_4^+ , HCO_3^- , and OH^- ions which locally change the pH of the solution. **Figure 9d** demonstrates the real-time response of the bio-FET to different concentrations of urea[81]. As the urea concentration increases, more charge carriers accumulate on the channel surface, which increases the drain current. Using a PASE-modified RGO, Chae et al. identified acetylcholine (ACh) neurotransmitter with a LOD of 1 μM [163]. In this work, acetylcholinesterase (AChE) was used as a probe and Ach-AChE enzymatic reaction leads to the accumulation of H^+ protons on the surface of RGO (**Figure 9e**).

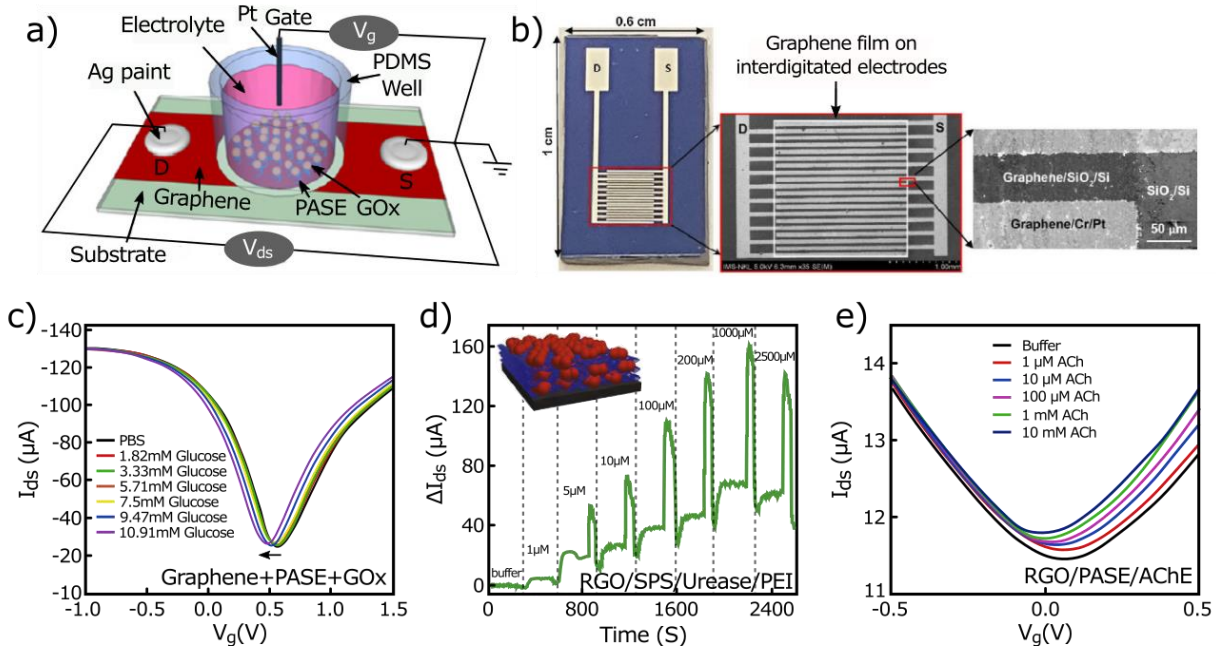


Figure 9. GFET enzymatic biosensors. **a)** Schematic illustration of a conventional bio-GFET[165]. **b)** Optical and SEM image of interdigitated electrodes containing graphene as an enzymatic bio-FETs[82]. **c)** I_{ds} - V_g characteristics of the GFET biosensor upon different concentrations of glucose[165]. **d)** Real-time response of the RGO biosensor to

various inlet urea concentrations from 1 μ M to 2500 μ M[81]. **e)** Transfer curve of the RGO biosensor in response to different concentrations of Ach biomolecules[163].

Enzymatic biosensors based on other 2D materials such as MoS₂ and WSe₂ have been also introduced up to date. Lee et al. employed mechanically exfoliated WSe₂ few layers to detect glucose in a range of 1 to 10 mM, with the help of APTES+GA and GOx as linkers and probes, respectively[167]. GA cross-linker is used as a middle-linker to facilitate an effective immobilization of GOx on WSe₂. **Figure 10a** presents a schematic of the biosensor, the corresponding configuration of the linkers and GOx, and photograph of the FET channel. Upon the enzymatic reactions, H⁺ ions and electrons are generated (**Figure 10b**) which electrons are directly transferred into the channel causing an n-doping effect as shown in **Figure 10c**. Shan et al. attached GOx directly on MoS₂ where detection of glucose was done by a similar procedure[168]. According to **Figure 10d**, as the glucose concentration increases, the drain current increases since more electrons transfer into the MoS₂.

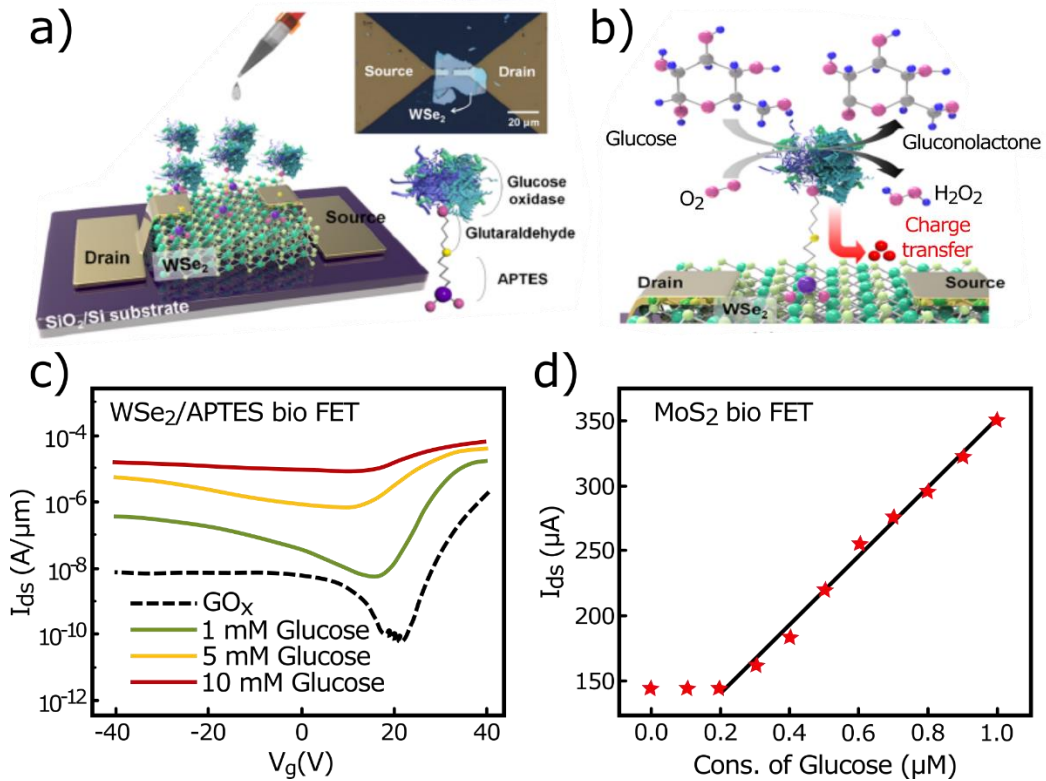


Figure 10. Beyond GFET enzymatic biosensors. **a)** Schematic illustration of a WSe₂ bio-FET with corresponding molecular configurations and image of the FET, **b)** Detection mechanism of the glucose near surface of the WSe₂ bio-FET, and **c)** its I_{ds} - V_g characteristics in response to three different glucose concentrations (1, 5, 10 mM)[167]. **d)** I_{ds} versus glucose concentrations in a MoS₂ bio-FET[168]. **e)** SEM image of the In₂O₃ bio-FET with a planar gate electrode, and **f)** real-time response to different concentrations of glucose from 10 nM to 1 mM[169].

Table 4 summarizes performance of the 2D-based FET enzymatic biosensor in identifying different biomolecules with relevant parameters.

Table 4. Performance summary of 2D based FET enzymatic biosensors in detection of various bio targets.

material	Target antigen	dynamic range	linker	gate electrode	electrolyte	LOD	sensing mechanism	ref
RGO	glucose	1 nM-100 mM	DMT-MM	Ag/AgCl	PBS	1 nM	gating	[164]
	urea	1-1000 μM	SPS	-	10 mM KCl	1 μM	gating	[81]
	ACh	1 μM- 10 mM	PASE	Ag/AgCl	0.1 mM PBS	1 μM	gating	[163]
Graphene	carbaryl	1.2 μM- 1.2 mM	GA	Ag/AgCl	Urea/water	0.1 fM	gating	[82]
	glucose	3.3-10.9 mM	PASE	Pt wire	PBS	3.3 mM	n-doping	[165]

glucose	0.5 μ M-1 mM	PtNPs	sensor	PBS	0.5 μ M	-	[166]	
Ach	5-1000 μ M	PABA	Ag/AgCl	KCl (10 mM) + HEPES (0.1 mM)	2.3 μ M	n-doping	[170]	
Lactose	1 aM- 1 nM	AuNPs	Ag wire	0.01×PBS	200 Am	n-doping	[171]	
MoS ₂	Glucose	300 nM-30 mM	Linker free	back-gated Si	0.1 mol/L PBS	300 nM	n-doping	[168]
WSe ₂	Glucose	1-10 mM	APTES	back-gated Si	Dry state	-	n-doping	[167]
In ₂ O ₃	Glucose	10 nM-1 mM	Chitosan	Planar Au	0.01×PBS	10 nM	gating	[169]

2. Bio-medical applications of FET biosensors

Bio-clinical diagnosis offers an innovative approach in monitoring human health status in everyday life. Most conventional methods depend on blood sampling because it provides rich information about blood urea, blood ions, glucose, and other parameters. However, this method is painful, time-consuming, and expensive. As a result, modern medicine desperately needs new solutions.

In addition to blood, the human body can produce other biofluids as clinical samples for disease detection. The human body secretes various biofluids such as tear, sweat, urine, saliva, and serum. All of these biofluids are evaluable as clinical samples for biosensing purposes. Salts, proteins, enzymes, and antibodies are found in the tear. In case of saliva, it contains various cells, enzymes, ions, and antibodies. Urine has glucose, proteins, cells, and bacteria. Sweat is composed of salt, proteins, bacteria, urea, ions, and other minerals and acids. Blood serum contains a variety of biomarkers, lipids, and salt. Therefore, FET biosensors have the advantage of being selective to detect bio targets via all human biofluids. Moreover, it can play a significant role in the future of bio-sensing technology by providing cheap, label-free, high-sensitive, high-selective, and real-time testing.

Up to now, most 2D-based bio-FET are tested in aqueous environments such as PBS at a pH value of 7.4. However, the term “point of care” for these types of biosensors can come true when they could operate accurately in real (clinical) samples. Fortunately, with the dramatic advancement of 2D materials, various 2D-based FET biosensors have gained the ability to real-time monitoring of disease in diluted clinical samples. In fact, human samples are usually diluted with buffer solutions due to their high viscosity[105].

To the best of our knowledge, 2D-based FET aptasensors have been employed to identify bio targets in different real samples such as urine, saliva, sweat, and serum. Hao et al. measured insulin in a diluted human urine sample with a LOD of 680 fM[91]. **Figure 11a** shows the change of drain current of the GFET aptasensor upon adding different insulin concentrations in human urine. The Dirac voltage shift of 10 healthy samples (called healthy control) and 10 patient samples (called hepatocellular carcinoma, HCC) that are collected from human serum are compared in **Figure 11b** for an RGO-based aptasensor[87]. Accordingly, the Dirac voltage shift is clearly detectable in patient samples compared to the healthy samples. In addition to urine and serum, other 2D based FET aptasensors have been introduced to diagnose biotargets in saliva[102, 105, 106] and sweat[71, 172].

In the case of 2D-based FET DNA biosensors, they are mostly tested in human serum samples. In fact, the cDNA (or RNA) is spiked into a diluted human serum and then added to the biosensor. **Figure 11c** shows the I_{ds} - V_g characteristic of a GFET DNA biosensor in a fresh serum and a serum containing 100 aM and 1 fM target RNAs[129]. Mei et al. demonstrated that the FET channel containing MoS_2 +probe DNA well responds to a serum with different concentrations of cDNA (**Figure 11d**)[125].

2D-based FET enzymatic biosensors have been successfully tested in different clinical samples such as saliva, serum, sweat, urine, and tear. Liu et al. employed In_2O_3 layer to detect glucose with

different concentrations in three clinical samples of saliva, artificial tear and artificial sweat[169].

Figure 11e shows the sensing response of the introduced FET upon these three samples compared to $0.1\times$ PBS. It is important to note that in addition to blood, glucose can be found in tears, sweat, and saliva but in lower concentrations[169]. Fenoy et al. spiked Ach in a urine sample and evaluated the FET biosensor's response to its different concentrations[170]. As shown in **Figure 11f**, stronger signals appear as the Ach concentration increases from $5\text{ }\mu\text{M}$ to 0.5 mM .

In addition to these types of FET biosensors, various 2D-based FET immunosensors have been reported based on real samples such as a nasopharyngeal swab, serum, and urine to detect disease. Yang et al. used a functionalized MoS_2 layer to identify NMP22 and CK8 biotargets as biomarkers of human bladder cancer in urine[173]. **Figure 11g** presents a schematic illustration of the identification process. Seo et al. utilized a GFET immunosensor to detect the SARS-CoV-2 virus in a diluted sample of the nasopharyngeal swabs[144]. **Figure 11h** shows the sensor response to a healthy sample and a patient sample containing the virus. In addition to urine and nasopharyngeal swab, some other 2D-based FET immunosensors have been tested in human serum samples. Chen et al. spiked different concentrations of the Ebola virus in human serum and tracked the change of I_{ds} per Ebola concentration[174].

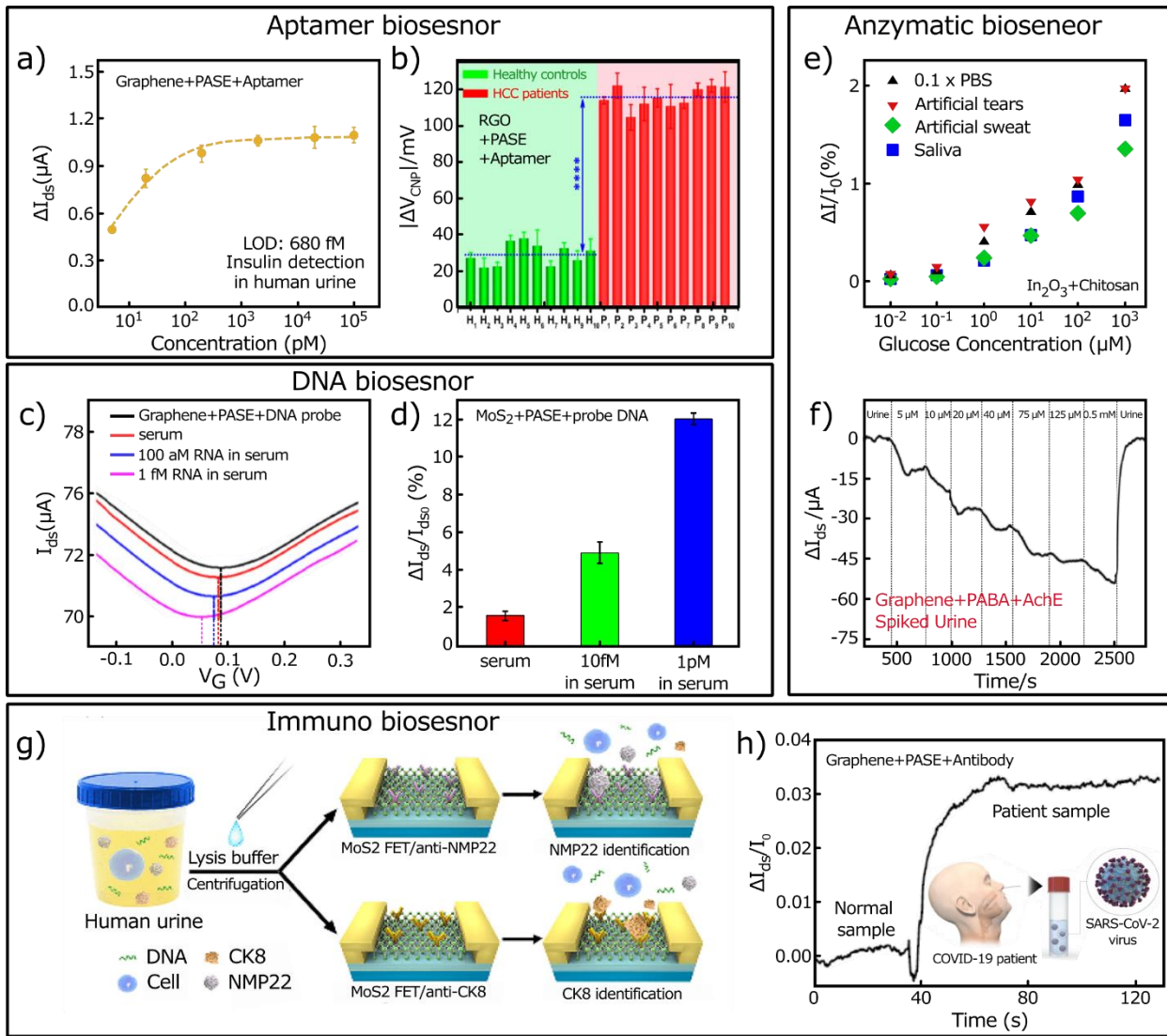


Figure 11. Performance of the 2D-based FET biosensors in clinical samples. **a)** GFET aptasensor response to different concentrations of insulin in human urine[91]. **b)** Comparison of RFET aptasensor response to 10 healthy and HCC patient samples collected from human serums[87]. **c)** Dirac voltage shift in a human serum containing 100 aM and 1 fM target RNA in a graphene-based DNA biosensor[129]. **d)** MoS₂ based DNA biosensor response to two different concentrations of target DNAs in human serum[125]. **e)** Performance of the In₂O₃ based enzymatic biosensor in detecting glucose under 0.1×PBS solution, artificial tear, artificial sweat and saliva[169]. **f)** Detection of spiked Ach biotarget in human urine by graphene-based enzymatic biosensor[170]. **g)** Detection process of NMP22 and CK8 biotargets in a MoS₂ based FET immunosensor[173]. **h)** Detection of SARS-CoV-2 virus in a patient's diluted nasopharyngeal swab sample via GFET immunosensor[144].

Table 5 summarizes the performance of the 2D-based FET biosensors to detect biotargets in different human samples of saliva, serum, sweat, urine, and tear. In some of them, the human biofluids directly contain biotargets[102, 105, 107, 173], but in others, certain biotargets are spiked

into them[175-178]. These FET biosensors show high accuracy and selectivity in identifying biotargets in real human samples. They can be used to diagnose or monitor diseases in the real world as promising POC devices for modern medicine.

Table 5. Performance of the 2D based FET biosensors in human clinical samples.

Bio-clinical sample	Bio probe	2D material	target	LOD	ref
Saliva and Nasopharyngeal swab*	Aptamer	RGO	HPV-16 E7	1.75 nM	[102]
		Graphene	CA1	-	[105]
	Immuno*	Graphene	IL-6	12.2 pM	[106]
		Graphene	SARS-CoV-2	0.01 fM	[144]
		In ₂ O ₃	Glucose	10 nM	[169]
Serum and blood	Aptamer	RGO+CNTs	CA125	-	[175]
		Graphene	IgE	47 pM	[178]
		Graphene	ADH	-	[177]
		Graphene	Cortisol	2.3 pM	[176]
		RGO	RNA	3.1 pM	[179]
	DNA	RGO	miRNA	10 fM	[118]
		Graphene	RNA	0.1 aM	[129]
		MoS ₂	DNA	6 fM	[125]
	immuno	MoS ₂	DNA	1 fM	[180]
		RGO	Ebola virus	0.2 fM	[174]
		RGO	CD63	-	[135]
		Graphene	BNP	100 fM	[64]
		MoS ₂	C-RP	0.06 fM	[147]
Sweat	immuno	MoS ₂	PSA	0.03 fM	[181]
		RGO	Glucose	1 nM	[164]
		Graphene	Cortisol	0.2 nM	[172]
	Enzyme	Graphene	INF-γ	740 fM	[71]
		In ₂ O ₃	Glucose	10 nM	[169]
Urine	Aptamer	Graphene	Insulin	680 fM	[91]
	Enzyme	Graphene	Ach	2.3 μM	[170]
	immuno	MoS ₂	NMP22	0.027 aM	[173]
			CK8	0.019 aM	
Tear	Enzyme	MoS ₂	glucose	-	[182]
		In ₂ O ₃	Glucose	10 nM	[169]

3. Conclusion and perspective

Early diagnosis of diseases is an important factor in reducing disease mortality. Among the various detection methods, FET-based biosensors have gained considerable potential in point of care diagnostics as on-site detection kits due to their high sensitivity, excellent selectivity, and rapid detection. In this review, a comprehensive report on 2D material-based bio-FETs is provided in which their performance in detecting a wide range of biospecies is thoroughly discussed. Commercial availability and high affinity of aptamers result in the implementation of many 2D-based aptamer and DNA FET biosensors, capable of detecting a variety of biomolecules and DNAs. The diversity of 2D-based FET immunosensors is larger than the other three categories and is expected to receive more attention in the future as viral diseases are constantly emerging. Among the four classified types, fewer reports have been published based on 2D-based FET enzymatic biosensors, perhaps due to the complexity of the detection process, in which target is usually measured indirectly based on the enzymatic reaction and ion release.

With recent advances in smart healthcare and wearable biosensors, reliable, fast, and noninvasive point of care devices like bio-FETs are urgently needed to accurately assess human health. As a result, modern medicine will rely more than ever on these point of care biosensors. Despite all these advantages, there are main challenges that need to be addressed to further develop 2D-based bio-FETs: 1) wide varieties of 2D materials have been explored up to now, the most important of which are Mxenes. However, a limited number of 2D materials have been so far introduced as 2D-based bio-FETs and there is a great place for the development of new 2D based bio-FETs. Before that, the biocompatibility of these new 2D materials should be investigated. 2) The wafer-scale growth of 2D materials needs to be highly developed than ever to make them more compatible with the silicon industry. 3) Stability, long-term toxicity, and reusability of 2D-based bio-FETs

should be carefully studied in-depth, and 4) more attention would be paid to the performance of 2D-based bio-FETs in the clinical samples in order to be commercially competitive.

Despite these challenges, 2D materials have much more to offer as biosensors. 2D materials show high surface area, excellent electrical conductivity, long-term chemical stability and good biocompatibility. Their integration in FET biosensors offers low detection limits, flexibility, real-time monitoring, label-free diagnosis and high selectivity. The 2D based bio-FETs promise development of new point of care testing devices which are suitable for future telemedicine. In addition, 2D bio-FETs are usually associated with a top-down fabrication approach that is more compatible with current technology. This area is at the beginning of the road and is expected to make significant progress in the near future. Altogether, 2D bio-FET can be one of the greatest medical achievements and soon its prominent role in human daily life will be seen.

References

- [1] A.E. Carmone, K. Kalaris, N. Leydon, N. Sirivansanti, J.M. Smith, A. Storey, A. Malata, Developing a common understanding of Networks of Care through a scoping study, *Health Systems & Reform*, 6 (2020) e1810921.
- [2] S. Morand, Emerging diseases, livestock expansion and biodiversity loss are positively related at global scale, *Biological Conservation*, 248 (2020) 108707.
- [3] Z. Zhou, X. Chen, H. Sheng, X. Shen, X. Sun, Y. Yan, J. Wang, Q. Yuan, Engineering probiotics as living diagnostics and therapeutics for improving human health, *Microbial Cell Factories*, 19 (2020) 1-12.
- [4] M. Locatelli, A. Tartaglia, F. D'Ambrosio, P. Ramundo, H. Ulusoy, K. Furton, A. Kabir, Biofluid sampler: A new gateway for mail-in-analysis of whole blood samples, *Journal of Chromatography B*, (2020) 122055.
- [5] D.B. Berry, E.K. Englund, S. Chen, L.R. Frank, S.R. Ward, Medical imaging of tissue engineering and regenerative medicine constructs, *Biomaterials Science*, (2020).
- [6] Z. He, Z. Chen, M. Tan, S. Elingarami, Y. Liu, T. Li, Y. Deng, N. He, S. Li, J. Fu, A review on methods for diagnosis of breast cancer cells and tissues, *Cell Proliferation*, (2020) e12822.
- [7] Z. Simmons, U. Ziemann, Terminology in neuromuscular electrodiagnostic medicine and ultrasound: Time for an update, *Muscle & Nerve*, (2020).
- [8] R. Hasterok, K. Wang, G. Jenkins, Progressive refinement of the karyotyping of *Brachypodium* genomes, *New Phytologist*, 227 (2020) 1668-1675.
- [9] H. Yang, H. Chen, B. Gao, W. Xiong, X. Zhang, D.K. Hogarth, J. Sun, M. Ke, F.J. Herth, Expert panel consensus statement on the applications and precaution strategies of bronchoscopy in patients with COVID-19, *Endoscopic Ultrasound*, 9 (2020) 211.
- [10] J. Zhao, W. Jiang, R. Zeng, *Physical Examination of Chest*, *Handbook of Clinical Diagnostics*, Springer2020, pp. 169-203.

[11] S.L. Sholapurkar, Intermittent auscultation (surveillance) of fetal heart rate in labor: a progressive evidence-backed approach with aim to improve methodology, reliability and safety, *The Journal of Maternal-Fetal & Neonatal Medicine*, (2020) 1-7.

[12] S. Iravani, Nano and biosensors for detection of SARS-CoV-2: challenges and opportunities, *Materials Advances*, (2020).

[13] S. Roy, S.J. Malode, N.P. Shetti, P. Chandra, Modernization of Biosensing Strategies for the Development of Lab-on-Chip Integrated Systems, *Bioelectrochemical Interface Engineering*, (2019) 325-342.

[14] F.S. Ligler, J.J. Gooding, Lighting up biosensors: Now and the decade to come, *Analytical chemistry*, 91 (2019) 8732-8738.

[15] H.D. Jirimali, Advance Biomedical Sensors and Transducers, *Biomedical Engineering and its Applications in Healthcare*, Springer2019, pp. 153-168.

[16] S.T. Shah, M. Khalid, R. Walvekar, N.M. Mubarak, Nanomaterial for Biosensors, *Advances in Nanotechnology and Its Applications*, Springer2020, pp. 35-61.

[17] S. Singh, V. Kumar, D.S. Dhanjal, S. Datta, R. Prasad, J. Singh, Biological biosensors for monitoring and diagnosis, *Microbial Biotechnology: Basic Research and Applications*, Springer2020, pp. 317-335.

[18] Y.S. Rim, Review of metal oxide semiconductors-based thin-film transistors for point-of-care sensor applications, *Journal of Information Display*, (2020) 1-8.

[19] C. Chen, J. Wang, Optical biosensors: an exhaustive and comprehensive review, *Analyst*, 145 (2020) 1605-1628.

[20] S.K. Metkar, K. Girigoswami, Diagnostic biosensors in medicine—A review, *Biocatalysis and Agricultural Biotechnology*, 17 (2019) 271-283.

[21] F. Otero, E. Magner, Biosensors—recent advances and future challenges in electrode materials, *Sensors*, 20 (2020) 3561.

[22] Q. Zhai, W. Cheng, Soft and stretchable electrochemical biosensors, *Materials Today Nano*, 7 (2019) 100041.

[23] D. Bahari, B. Babamiri, A. Salimi, R. Hallaj, S.M. Amininasab, A self-enhanced ECL-RET immunosensor for the detection of CA19-9 antigen based on Ru(bpy)2(phen-NH2)2⁺ - Amine-rich nitrogen-doped carbon nanodots as probe and graphene oxide grafted hyperbranched aromatic polyamide as platform, *Analytica Chimica Acta*, 1132 (2020) 55-65.

[24] A. Salimi, B. Kavosi, A. Navaee, Amine-functionalized graphene as an effective electrochemical platform toward easily miRNA hybridization detection, *Measurement*, 143 (2019) 191-198.

[25] M.C. Castrovilli, P. Bolognesi, J. Chiarinelli, L. Avaldi, P. Calandra, A. Antonacci, V. Scognamiglio, The convergence of forefront technologies in the design of laccase-based biosensors—An update, *TrAC Trends in Analytical Chemistry*, 119 (2019) 115615.

[26] K. Kivirand, M. Min, T. Rinken, Challenges and Applications of Impedance-Based Biosensors in Water Analysis, *Environmental Biosensors*, IntechOpen2019.

[27] Y. Matos-Peralta, M. Antuch, D.G. Abradelo, L. Bazán-Bravo, K.R. de la Luz Hernández, Glutamate Dehydrogenase-Based Electrochemical Biosensors: The Immobilization Method Defines Sensor Selectivity, *Journal of The Electrochemical Society*, 166 (2019) B1146.

[28] Y. Zhang, X. Chen, Nanotechnology and nanomaterial-based no-wash electrochemical biosensors: from design to application, *Nanoscale*, 11 (2019) 19105-19118.

[29] S. Anand, A. Singh, S.I. Amin, A.S. Thool, Design and performance analysis of dielectrically modulated doping-less tunnel FET-based label free biosensor, *IEEE Sensors Journal*, 19 (2019) 4369-4374.

[30] J. Luo, S. Li, M. Xu, M. Guan, M. Yang, J. Ren, Y. Zhang, Y. Zeng, Real-time detection of cardiac troponin I and mechanism analysis of AlGaAs/GaAs high electron mobility transistor biosensor, *AIP Advances*, 10 (2020) 115205.

[31] S. Park, J. Choi, M. Jeun, Y. Kim, S.S. Yuk, S.K. Kim, C.S. Song, S. Lee, K.H. Lee, Detection of avian influenza virus from cloacal swabs using a disposable well gate FET sensor, *Advanced Healthcare Materials*, 6 (2017) 1700371.

[32] N.N. Reddy, D.K. Panda, A comprehensive review on tunnel field-effect transistor (TFET) based biosensors: recent advances and future prospects on device structure and sensitivity, *Silicon*, (2020) 1-16.

[33] C. Rodriguez, P. Dietrich, V. Torres-Costa, V. Cebrián, C. Gómez-Abad, A. Díaz, O. Ahumada, M.M. Silván, Near ambient pressure X-ray photoelectron spectroscopy monitoring of the surface immobilization cascade on a porous silicon-gold nanoparticle FET biosensor, *Applied Surface Science*, 492 (2019) 362-368.

[34] T. Wadhera, D. Kakkar, G. Wadhwa, B. Raj, Recent advances and progress in development of the field effect transistor biosensor: A review, *Journal of Electronic Materials*, 48 (2019) 7635-7646.

[35] N. Masurkar, S. Varma, L. Mohana Reddy Arava, Supported and suspended 2D material-based FET biosensors, *Electrochem*, 1 (2020) 260-277.

[36] S. Chen, K. Yang, X. Leng, M. Chen, K.S. Novoselov, D.V. Andreeva, Perspectives in the design and application of composites based on graphene derivatives and bio-based polymers, *Polymer International*, 69 (2020) 1173-1186.

[37] S. Ebrahimi, Z.E. Nataj, S. Khodaverdian, A. Khamsavi, Y. Abdi, K. Khajeh, An ion-sensitive field-effect transistor biosensor based on SWCNT and aligned MWCNTs for detection of ABTS, *IEEE Sensors Journal*, (2020).

[38] S. Veeralingam, S. Badhulika, Surface functionalized β -Bi₂O₃ nanofibers based flexible, field-effect transistor-biosensor (BioFET) for rapid, label-free detection of serotonin in biological fluids, *Sensors and Actuators B: Chemical*, 321 (2020) 128540.

[39] C.-A. Vu, W.-P. Hu, Y.-S. Yang, H.W.-H. Chan, W.-Y. Chen, Signal Enhancement of Silicon Nanowire Field-Effect Transistor Immunosensors by RNA Aptamer, *ACS omega*, 4 (2019) 14765-14771.

[40] K.S. Novoselov, A.K. Geim, S.V. Morozov, D. Jiang, Y. Zhang, S.V. Dubonos, I.V. Grigorieva, A.A. Firsov, Electric field effect in atomically thin carbon films, *science*, 306 (2004) 666-669.

[41] Y. Seekaew, C. Wongchoosuk, A novel graphene-based electroluminescent gas sensor for carbon dioxide detection, *Applied Surface Science*, 479 (2019) 525-531.

[42] H. Song, X. Zhang, Y. Liu, Z. Su, Developing Graphene-Based Nanohybrids for Electrochemical Sensing, *The Chemical Record*, 19 (2019) 534-549.

[43] F. Wang, Y. Zhang, Y. Gao, P. Luo, J. Su, W. Han, K. Liu, H. Li, T. Zhai, 2D metal chalcogenides for IR photodetection, *Small*, 15 (2019) 1901347.

[44] L. Pi, L. Li, K. Liu, Q. Zhang, H. Li, T. Zhai, Recent Progress on 2D Noble-Transition-Metal Dichalcogenides, *Advanced Functional Materials*, 29 (2019) 1904932.

[45] J. Dai, M. Li, X.C. Zeng, Group IVB transition metal trichalcogenides: a new class of 2D layered materials beyond graphene, *Wiley Interdisciplinary Reviews: Computational Molecular Science*, 6 (2016) 211-222.

[46] X. Qi, Y. Zhang, Q. Ou, S.T. Ha, C.W. Qiu, H. Zhang, Y.B. Cheng, Q. Xiong, Q. Bao, Photonics and optoelectronics of 2D metal-halide perovskites, *Small*, 14 (2018) 1800682.

[47] N.R. Glavin, R. Rao, V. Varshney, E. Bianco, A. Apte, A. Roy, E. Ringe, P.M. Ajayan, Emerging applications of elemental 2D materials, *Advanced Materials*, 32 (2020) 1904302.

[48] J. Azadmanjiri, P. Kumar, V.K. Srivastava, Z. Sofer, Surface Functionalization of 2D Transition Metal Oxides and Dichalcogenides via Covalent and Non-covalent Bonding for Sustainable Energy and Biomedical Applications, *ACS Applied Nano Materials*, 3 (2020) 3116-3143.

[49] T. Wang, H. Wang, Z. Kou, W. Liang, X. Luo, F. Verpoort, Y.J. Zeng, H. Zhang, Xenes as an Emerging 2D Monoelemental Family: Fundamental Electrochemistry and Energy Applications, *Advanced Functional Materials*, 30 (2020) 2002885.

[50] Z. Li, X. Yin, Y. Sun, L. Qu, D. Du, Y. Lin, Functionalized Two-Dimensional Nanomaterials for Biosensing and Bioimaging, *Adapting 2D Nanomaterials for Advanced Applications*, ACS Publications2020, pp. 143-165.

[51] E.P. Nguyen, C.d.C.C. Silva, A. Merkoçi, Recent advancement in biomedical applications on the surface of two-dimensional materials: from biosensing to tissue engineering, *Nanoscale*, 12 (2020) 19043-19067.

[52] N. Rohaizad, C.C. Mayorga-Martinez, M. Fojtů, N.M. Latiff, M. Pumera, Two-dimensional materials in biomedical, biosensing and sensing applications, *Chemical Society Reviews*, (2020).

[53] D. Sadighbayan, M. Hasanzadeh, E. Ghafar-Zadeh, Biosensing based on field-effect transistors (FET): Recent progress and challenges, *TrAC Trends in Analytical Chemistry*, (2020) 116067.

[54] S. Mansouri Majd, F. Ghasemi, A. Salimi, T.-K. Sham, Transport Properties of a Molybdenum Disulfide and Carbon Dot Nanohybrid Transistor and Its Applications as a Hg²⁺ Aptasensor, *ACS Applied Electronic Materials*, 2 (2020) 635-645.

[55] R. Campos, J.r.m. Borme, J.R. Guerreiro, G. Machado Jr, M.F.t. Cerqueira, D.Y. Petrovykh, P. Alpuim, Attomolar label-free detection of DNA hybridization with electrolyte-gated graphene field-effect transistors, *ACS sensors*, 4 (2019) 286-293.

[56] J. Kwon, B.-H. Lee, S.-Y. Kim, J.-Y. Park, H. Bae, Y.-K. Choi, J.-H. Ahn, Nanoscale FET-based transduction toward sensitive extended-gate biosensors, *ACS sensors*, 4 (2019) 1724-1729.

[57] M. Tian, Z. Li, R. Song, Y. Li, C. Guo, Y. Sha, W. Cui, S. Xu, G. Hu, J. Wang, Graphene biosensor as affinity biosensors for biorecognition between Guanine riboswitch and ligand, *Applied Surface Science*, 503 (2020) 144303.

[58] T.-T. Tran, K. Clark, W. Ma, A. Mulchandani, Detection of a secreted protein biomarker for citrus Huanglongbing using a single-walled carbon nanotubes-based chemiresistive biosensor, *Biosensors and Bioelectronics*, 147 (2020) 111766.

[59] F. Chen, Q. Qing, J. Xia, N. Tao, Graphene Field-Effect Transistors: Electrochemical Gating, Interfacial Capacitance, and Biosensing Applications, *Chemistry—An Asian Journal*, 5 (2010) 2144-2153.

[60] K.D. Dorfman, D.Z. Adrahas, M.S. Thomas, C.D. Frisbie, Microfluidic opportunities in printed electrolyte-gated transistor biosensors, *Biomicrofluidics*, 14 (2020) 011301.

[61] I. Novodchuk, M. Bajcsy, M. Yavuz, Graphene-Based Field Effect Transistor Biosensors for Breast Cancer Detection: A Review on Biosensing Strategies, *Carbon*, (2020).

[62] X. Dong, Y. Shi, W. Huang, P. Chen, L.-J. Li, Electrical Detection of DNA Hybridization with Single-Base Specificity Using Transistors Based on CVD-Grown Graphene Sheets, *Advanced Materials*, 22 (2010) 1649-1653.

[63] S. Ghosh, N.I. Khan, J.G. Tsavalas, E. Song, Selective Detection of Lysozyme Biomarker Utilizing Large Area Chemical Vapor Deposition-Grown Graphene-Based Field-Effect Transistor, *Frontiers in Bioengineering and Biotechnology*, 6 (2018).

[64] Y.-M. Lei, M.-M. Xiao, Y.-T. Li, L. Xu, H. Zhang, Z.-Y. Zhang, G.-J. Zhang, Detection of heart failure-related biomarker in whole blood with graphene field effect transistor biosensor, *Biosensors and Bioelectronics*, 91 (2017) 1-7.

[65] Z. Wang, Z. Hao, S. Yu, C. Huang, Y. Pan, X. Zhao, A Wearable and Deformable Graphene-Based Affinity Nanosensor for Monitoring of Cytokines in Biofluids, *Nanomaterials*, 10 (2020) 1503.

[66] Z. Gao, H. Xia, J. Zauberman, M. Tomaiuolo, J. Ping, Q. Zhang, P. Ducos, H. Ye, S. Wang, X. Yang, F. Lubna, Z. Luo, L. Ren, A.T.C. Johnson, Detection of Sub-fM DNA with Target Recycling and Self-Assembly Amplification on Graphene Field-Effect Biosensors, *Nano Letters*, 18 (2018) 3509-3515.

[67] G. Wu, Z. Dai, X. Tang, Z. Lin, P.K. Lo, M. Meyyappan, K.W.C. Lai, Graphene Field-Effect Transistors for the Sensitive and Selective Detection of *Escherichia coli* Using Pyrene-Tagged DNA Aptamer, *Advanced Healthcare Materials*, 6 (2017) 1700736.

[68] A. Schuck, H.E. Kim, K.-M. Jung, W. Hasenkamp, Y.-S. Kim, Monitoring the hemostasis process through the electrical characteristics of a graphene-based field-effect transistor, *Biosensors and Bioelectronics*, (2020) 112167.

[69] S. Kalra, M.J. Kumar, A. Dhawan, Reconfigurable FET Biosensor for a Wide Detection Range and Electrostatically Tunable Sensing Response, *IEEE Sensors Journal*, 20 (2019) 2261-2269.

[70] O. Oshin, D. Kireev, H. Hlukhova, F. Idachaba, D. Akinwande, A. Atayero, Graphene-based biosensor for early detection of iron deficiency, *Sensors*, 20 (2020) 3688.

[71] Z. Wang, Z. Hao, X. Wang, C. Huang, Q. Lin, X. Zhao, Y. Pan, A Flexible and Regenerative Aptameric Graphene–Nafion Biosensor for Cytokine Storm Biomarker Monitoring in Undiluted Biofluids toward Wearable Applications, *Advanced Functional Materials*, (2020) 2005958.

[72] S.K. Sailapu, E. Macchia, I. Merino-Jimenez, J.P. Esquivel, L. Sarcina, G. Scamarcio, S.D. Minteer, L. Torsi, N. Sabaté, Standalone operation of an EGOFET for ultra-sensitive detection of HIV, *Biosensors and Bioelectronics*, 156 (2020) 112103.

[73] L. Zhou, K. Wang, H. Sun, S. Zhao, X. Chen, D. Qian, H. Mao, J. Zhao, Novel Graphene Biosensor Based on the Functionalization of Multifunctional Nano-bovine Serum Albumin for the Highly Sensitive Detection of Cancer Biomarkers, *Nano-Micro Letters*, 11 (2019) 20.

[74] C. Zhan, J. Neal, J. Wu, D.-e. Jiang, Quantum effects on the capacitance of graphene-based electrodes, *The Journal of Physical Chemistry C*, 119 (2015) 22297-22303.

[75] S. Rosenblatt, Y. Yaish, J. Park, J. Gore, V. Sazonova, P.L. McEuen, High performance electrolyte gated carbon nanotube transistors, *Nano letters*, 2 (2002) 869-872.

[76] I. Sarangadharan, S.-L. Wang, T.-Y. Tai, A.K. Pulikkathodi, C.-P. Hsu, H.-H.K. Chiang, L.Y.-M. Liu, Y.-L. Wang, Risk stratification of heart failure from one drop of blood using hand-held biosensor for BNP detection, *Biosensors and Bioelectronics*, 107 (2018) 259-265.

[77] J. Huang, Confinement Induced Dilution: Electrostatic Screening Length Anomaly in Concentrated Electrolytes in Confined Space, *The Journal of Physical Chemistry C*, 122 (2018) 3428-3433.

[78] I.M. Bhattacharyya, G. Shalev, Electrostatically Governed Debye Screening Length at the Solution-Solid Interface for Biosensing Applications, *ACS sensors*, 5 (2019) 154-161.

[79] P. Didier, T. Minami, Non-enzymatic lactate detection by an extended-gate type organic field effect transistor, *Semiconductor Science and Technology*, 35 (2020) 11LT02.

[80] F. Khosravi-Nejad, M. Teimouri, S.J. Marandi, M. Shariati, The highly sensitive impedimetric biosensor in label free approach for hepatitis B virus DNA detection based on tellurium doped ZnO nanowires, *Applied Physics A*, 125 (2019) 616.

[81] E. Piccinini, C. Bliem, C. Reiner-Rozman, F. Battaglini, O. Azzaroni, W. Knoll, Enzyme-polyelectrolyte multilayer assemblies on reduced graphene oxide field-effect transistors for biosensing applications, *Biosensors and Bioelectronics*, 92 (2017) 661-667.

[82] C.T. Thanh, N.H. Binh, N. Van Tu, V.T. Thu, M. Bayle, M. Paillet, J.L. Sauvajol, P.B. Thang, T.D. Lam, P.N. Minh, N. Van Chuc, An interdigitated ISFET-type sensor based on LPCVD grown graphene for ultrasensitive detection of carbaryl, *Sensors and Actuators B: Chemical*, 260 (2018) 78-85.

[83] E. Stern, R. Wagner, F.J. Sigworth, R. Breaker, T.M. Fahmy, M.A. Reed, Importance of the Debye Screening Length on Nanowire Field Effect Transistor Sensors, *Nano Letters*, 7 (2007) 3405-3409.

[84] M. Choi, J. Heo, H. Kim, S.W. Kang, J. Hong, Control of gas permeability by transforming the molecular structure of silk fibroin in multilayered nanocoatings for CO₂ adsorptive separation, *Journal of Membrane Science*, 573 (2019) 554-559.

[85] L. Wang, C. Zhang, T. Li, M. Duan, F. Xia, X. Li, C. Song, S. Pan, B. Liu, D. Cui, A modular approach for cytosolic protein delivery: metal ion-induced self-assembly of gold nanoclusters as a general platform, *Nanoscale*, 11 (2019) 22237-22242.

[86] C.-A. Vu, W.-Y. Chen, Predicting Future Prospects of Aptamers in Field-Effect Transistor Biosensors, *Molecules*, 25 (2020) 680.

[87] D. Wu, Y. Yu, D. Jin, M.-M. Xiao, Z.-Y. Zhang, G.-J. Zhang, Dual-Aptamer Modified Graphene Field-Effect Transistor Nanosensor for Label-Free and Specific Detection of Hepatocellular Carcinoma-Derived Microvesicles, *Analytical Chemistry*, 92 (2020) 4006-4015.

[88] S. Farid, X. Meshik, M. Choi, S. Mukherjee, Y. Lan, D. Parikh, S. Poduri, U. Baterdene, C.-E. Huang, Y.Y. Wang, P. Burke, M. Dutta, M.A. Stroscio, Detection of Interferon gamma using graphene and aptamer based FET-like electrochemical biosensor, *Biosensors and Bioelectronics*, 71 (2015) 294-299.

[89] Z. Jiang, B. Feng, J. Xu, T. Qing, P. Zhang, Z. Qing, Graphene biosensors for bacterial and viral pathogens, *Biosensors and Bioelectronics*, 166 (2020) 112471.

[90] S.Y. Tan, C. Acquah, A. Sidhu, C.M. Ongkudon, L.S. Yon, M.K. Danquah, SELEX Modifications and Bioanalytical Techniques for Aptamer–Target Binding Characterization, *Critical Reviews in Analytical Chemistry*, 46 (2016) 521-537.

[91] Z. Hao, Y. Pan, C. Huang, Z. Wang, Q. Lin, X. Zhao, S. Liu, Modulating the Linker Immobilization Density on Aptameric Graphene Field Effect Transistors Using an Electric Field, *ACS Sensors*, 5 (2020) 2503-2513.

[92] N. Nekrasov, D. Kireev, A. Emelianov, I. Bobrinetskiy, Graphene-Based Sensing Platform for On-Chip Ochratoxin A Detection, *Toxins*, 11 (2019) 550.

[93] Z. Hao, Y. Zhu, X. Wang, P.G. Rotti, C. DiMarco, S.R. Tyler, X. Zhao, J.F. Engelhardt, J. Hone, Q. Lin, Real-Time Monitoring of Insulin Using a Graphene Field-Effect Transistor Aptamer Nanosensor, *ACS Applied Materials & Interfaces*, 9 (2017) 27504-27511.

[94] X. Chen, S. Hao, B. Zong, C. Liu, S. Mao, Ultraselective antibiotic sensing with complementary strand DNA assisted aptamer/MoS₂ field-effect transistors, *Biosensors and Bioelectronics*, 145 (2019) 111711.

[95] D.J. Kim, H.C. Park, I.Y. Sohn, J.H. Jung, O.J. Yoon, J.S. Park, M.Y. Yoon, N.E. Lee, Electrical Graphene Aptasensor for Ultra-Sensitive Detection of Anthrax Toxin with Amplified Signal Transduction, *Small*, 9 (2013) 3352-3360.

[96] Y. Duan, Y. Yang, J. Wang, H. Li, K. Liu, A facile one-pot synthesis of polyethyleneimine functionalized graphene for the highly-sensitive and selective electrochemical impedance aptasensing of kanamycin in serum, *Analytical Methods*, 12 (2020) 132-140.

[97] Y. Yang, X. Yang, X. Zou, S. Wu, D. Wan, A. Cao, L. Liao, Q. Yuan, X. Duan, Ultrafine graphene nanomesh with large on/off ratio for high-performance flexible biosensors, *Advanced Functional Materials*, 27 (2017) 1604096.

[98] R. Singh, S. Sansare, S. Shidhaye, Biomedical application of graphenes, *Biomedical Applications of Nanoparticles*, Elsevier2019, pp. 319-339.

[99] M. Begić, D. Josić, Biofilm formation and extracellular microvesicles—The way of foodborne pathogens toward resistance, *Electrophoresis*, 41 (2020) 1718-1739.

[100] C.A. Whitehead, A.H. Kaye, K.J. Drummond, S.S. Widodo, T. Mantamadiotis, L.J. Vella, S.S. Stylli, Extracellular vesicles and their role in glioblastoma, *Critical reviews in clinical laboratory sciences*, 57 (2020) 227-252.

[101] H. Park, S. Baek, B. Jeong, S. Kim, Y.C. Park, S. Kim, Nanomesh-patterning on multilayer MoS₂ field-effect transistors for ultra-sensitive detection of cortisol, (2020).

[102] P. Aspermair, V. Mishyn, J. Bintinger, H. Happy, K. Bagga, P. Subramanian, W. Knoll, R. Boukherroub, S. Szunerits, Reduced graphene oxide-based field effect transistors for the detection of E7 protein of human papillomavirus in saliva, *Analytical and Bioanalytical Chemistry*, 413 (2021) 779-787.

[103] N.I. Khan, M. Mousazadehkasin, S. Ghosh, J.G. Tsavalas, E. Song, An integrated microfluidic platform for selective and real-time detection of thrombin biomarkers using a graphene FET, *Analyst*, 145 (2020) 4494-4503.

[104] N.I. Khan, E. Song, Detection of an IL-6 Biomarker Using a GFET Platform Developed with a Facile Organic Solvent-Free Aptamer Immobilization Approach, *Sensors*, 21 (2021) 1335.

[105] N. Kumar, M. Gray, J.C. Ortiz-Marquez, A. Weber, C.R. Desmond, A. Argun, T. van Opijken, K.S. Burch, Detection of a multi-disease biomarker in saliva with graphene field effect transistors, *MEDICAL DEVICES & SENSORS*, 3 (2020) e10121.

[106] Z. Hao, Y. Pan, W. Shao, Q. Lin, X. Zhao, Graphene-based fully integrated portable nanosensing system for on-line detection of cytokine biomarkers in saliva, *Biosensors and Bioelectronics*, 134 (2019) 16-23.

[107] M. Vasudevan, M.J. Tai, V. Perumal, S.C. Gopinath, S.S. Murthe, M. Ovinis, N.M. Mohamed, N. Joshi, Highly sensitive and selective acute myocardial infarction detection using aptamer-tethered MoS2 nanoflower and screen-printed electrodes, *Biotechnology and Applied Biochemistry*, (2020).

[108] B. Cai, S. Wang, L. Huang, Y. Ning, Z. Zhang, G.-J. Zhang, Ultrasensitive Label-Free Detection of PNA–DNA Hybridization by Reduced Graphene Oxide Field-Effect Transistor Biosensor, *ACS Nano*, 8 (2014) 2632-2638.

[109] Y. Chen, Y. Li, H. Chao, J. Wu, W. Zhu, T. Fang, X. Gao, D. Yan, Molecular cloning and characterisation of a novel xanthine oxidase from *Cellulosimicrobium cellulans* ATCC21606, *Process Biochemistry*, 91 (2020) 65-72.

[110] C. Li, H. Li, J. Ge, G. Jie, Versatile fluorescence detection of microRNA based on novel DNA hydrogel-amplified signal probes coupled with DNA walker amplification, *Chemical Communications*, 55 (2019) 3919-3922.

[111] S. Zhou, T. Gou, J. Hu, W. Wu, X. Ding, W. Fang, Z. Hu, Y. Mu, A highly integrated real-time digital PCR device for accurate DNA quantitative analysis, *Biosensors and Bioelectronics*, 128 (2019) 151-158.

[112] D.-W. Lee, J. Lee, I.Y. Sohn, B.-Y. Kim, Y.M. Son, H. Bark, J. Jung, M. Choi, T.H. Kim, C. Lee, Field-effect transistor with a chemically synthesized MoS 2 sensing channel for label-free and highly sensitive electrical detection of DNA hybridization, *Nano Research*, 8 (2015) 2340-2350.

[113] C.T. Lin, P.T.K. Loan, T.Y. Chen, K.K. Liu, C.H. Chen, K.H. Wei, L.J. Li, Label-Free Electrical detection of DNA hybridization on graphene using Hall Effect measurements: revisiting the sensing mechanism, *Advanced Functional Materials*, 23 (2013) 2301-2307.

[114] N. Mudgal, A. Saharia, K.K. Choure, A. Agarwal, G. Singh, Sensitivity enhancement with anti-reflection coating of silicon nitride (Si 3 N 4) layer in silver-based Surface Plasmon Resonance (SPR) sensor for sensing of DNA hybridization, *Applied Physics A*, 126 (2020) 1-8.

[115] M.D. Verona, V. Verdolino, F. Palazzi, R. Corradini, Focus on PNA Flexibility and RNA binding using molecular dynamics and metadynamics, *Scientific reports*, 7 (2017) 42799.

[116] Z. Gao, H. Kang, C.H. Naylor, F. Streller, P. Ducos, M.D. Serrano, J. Ping, J. Zauberman, Rajesh, R.W. Carpick, Y.-J. Wang, Y.W. Park, Z. Luo, L. Ren, A.T.C. Johnson, Scalable Production of Sensor Arrays Based on High-Mobility Hybrid Graphene Field Effect Transistors, *ACS Applied Materials & Interfaces*, 8 (2016) 27546-27552.

[117] J. Ping, R. Vishnubhotla, A. Vrudhula, A.T.C. Johnson, Scalable Production of High-Sensitivity, Label-Free DNA Biosensors Based on Back-Gated Graphene Field Effect Transistors, *ACS Nano*, 10 (2016) 8700-8704.

[118] B. Cai, L. Huang, H. Zhang, Z. Sun, Z. Zhang, G.-J. Zhang, Gold nanoparticles-decorated graphene field-effect transistor biosensor for femtomolar MicroRNA detection, *Biosensors and Bioelectronics*, 74 (2015) 329-334.

[119] Z. Yin, Q. He, X. Huang, J. Zhang, S. Wu, P. Chen, G. Lu, Q. Zhang, Q. Yan, H. Zhang, Real-time DNA detection using Pt nanoparticle-decorated reduced graphene oxide field-effect transistors, *Nanoscale*, 4 (2012) 293-297.

[120] Y. Tu, X. Wang, Recent Advances in Cell Adhesive Force Microscopy, *Sensors*, 20 (2020) 7128.

[121] C. Zheng, L. Huang, H. Zhang, Z. Sun, Z. Zhang, G.-J. Zhang, Fabrication of ultrasensitive field-effect transistor DNA biosensors by a directional transfer technique based on CVD-grown graphene, *ACS applied materials & interfaces*, 7 (2015) 16953-16959.

[122] Z. Wang, Y. Jia, Graphene solution-gated field effect transistor DNA sensor fabricated by liquid exfoliation and double glutaraldehyde cross-linking, *Carbon*, 130 (2018) 758-767.

[123] S. Xu, J. Zhan, B. Man, S. Jiang, W. Yue, S. Gao, C. Guo, H. Liu, Z. Li, J. Wang, Real-time reliable determination of binding kinetics of DNA hybridization using a multi-channel graphene biosensor, *Nature communications*, 8 (2017) 14902.

[124] J. Liu, X. Chen, Q. Wang, M. Xiao, D. Zhong, W. Sun, G. Zhang, Z. Zhang, Ultrasensitive Monolayer MoS₂ Field-Effect Transistor Based DNA Sensors for Screening of Down Syndrome, *Nano Letters*, 19 (2019) 1437-1444.

[125] J. Mei, Y.-T. Li, H. Zhang, M.-M. Xiao, Y. Ning, Z.-Y. Zhang, G.-J. Zhang, Molybdenum disulfide field-effect transistor biosensor for ultrasensitive detection of DNA by employing morpholino as probe, *Biosensors and Bioelectronics*, 110 (2018) 71-77.

[126] P. Kanyong, A.V. Patil, J.J. Davis, Functional Molecular Interfaces for Impedance-Based Diagnostics, *Annual Review of Analytical Chemistry*, 13 (2020) 183-200.

[127] S. Xu, S. Jiang, C. Zhang, W. Yue, Y. Zou, G. Wang, H. Liu, X. Zhang, M. Li, Z. Zhu, J. Wang, Ultrasensitive label-free detection of DNA hybridization by sapphire-based graphene field-effect transistor biosensor, *Applied Surface Science*, 427 (2018) 1114-1119.

[128] R. Song, M. Tian, Y. Li, J. Liu, G. Liu, S. Xu, J. Wang, Detection of MicroRNA Based on Three-Dimensional Graphene Field-Effect Transistor Biosensor, *Nano*, 15 (2020) 2050039.

[129] M. Tian, M. Qiao, C. Shen, F. Meng, L.A. Frank, V.V. Krasitskaya, T. Wang, X. Zhang, R. Song, Y. Li, J. Liu, S. Xu, J. Wang, Highly-sensitive graphene field effect transistor biosensor using PNA and DNA probes for RNA detection, *Applied Surface Science*, 527 (2020) 146839.

[130] M.T. Hwang, M. Heiranian, Y. Kim, S. You, J. Leem, A. Taqieddin, V. Faramarzi, Y. Jing, I. Park, A.M. van der Zande, S. Nam, N.R. Aluru, R. Bashir, Ultrasensitive detection of nucleic acids using deformed graphene channel field effect biosensors, *Nature Communications*, 11 (2020) 1543.

[131] S. Chen, Y. Sun, Y. Xia, K. Lv, B. Man, C. Yang, Donor effect dominated molybdenum disulfide/graphene nanostructure-based field-effect transistor for ultrasensitive DNA detection, *Biosensors and Bioelectronics*, 156 (2020) 112128.

[132] D.-J. Kim, I.Y. Sohn, J.-H. Jung, O.J. Yoon, N.E. Lee, J.-S. Park, Reduced graphene oxide field-effect transistor for label-free femtomolar protein detection, *Biosensors and Bioelectronics*, 41 (2013) 621-626.

[133] S. Mao, K. Yu, J. Chang, D.A. Steeber, L.E. Ocola, J. Chen, Direct Growth of Vertically-oriented Graphene for Field-Effect Transistor Biosensor, *Scientific Reports*, 3 (2013) 1696.

[134] B. Thakur, G. Zhou, J. Chang, H. Pu, B. Jin, X. Sui, X. Yuan, C.-H. Yang, M. Magruder, J. Chen, Rapid detection of single *E. coli* bacteria using a graphene-based field-effect transistor device, *Biosensors and Bioelectronics*, 110 (2018) 16-22.

[135] Y. Yu, Y.-T. Li, D. Jin, F. Yang, D. Wu, M.-M. Xiao, H. Zhang, Z.-Y. Zhang, G.-J. Zhang, Electrical and Label-Free Quantification of Exosomes with a Reduced Graphene Oxide Field Effect Transistor Biosensor, *Analytical Chemistry*, 91 (2019) 10679-10686.

[136] N. Bohli, M. Belkilani, L. Mora, A. Abdelghani, Antibody-functionalised gold nanoparticles-based impedimetric immunosensor: Detection methods for better sensitivity, *Micro & Nano Letters*, 14 (2019) 629-633.

[137] X. Deng, Y. Nakamura, Cancer precision medicine: from cancer screening to drug selection and personalized immunotherapy, *Trends in pharmacological sciences*, 38 (2017) 15-24.

[138] Z. Gao, P. Ducos, H. Ye, J. Zauberman, A. Sriram, X. Yang, Z. Wang, M.W. Mitchell, D. Lekkas, D. Brisson, A.T.C. Johnson, Graphene transistor arrays functionalized with genetically engineered antibody fragments for Lyme disease diagnosis, *2D Materials*, 7 (2020) 024001.

[139] C. Haslam, S. Damiati, T. Whitley, P. Davey, E. Ifeatchor, S.A. Awan, Label-free sensors based on graphene field-effect transistors for the detection of human chorionic gonadotropin cancer risk biomarker, *Diagnostics*, 8 (2018) 5.

[140] J.H. Jung, I.Y. Sohn, D.J. Kim, B.Y. Kim, M. Jang, N.-E. Lee, Enhancement of protein detection performance in field-effect transistors with polymer residue-free graphene channel, *Carbon*, 62 (2013) 312-321.

[141] D. Kwong Hong Tsang, T.J. Lieberthal, C. Watts, I.E. Dunlop, S. Ramadan, A.E. del Rio Hernandez, N. Klein, Chemically Functionalised Graphene FET Biosensor for the Label-free Sensing of Exosomes, *Scientific Reports*, 9 (2019) 13946.

[142] Rajesh, Z. Gao, R. Vishnubhotla, P. Ducos, M.D. Serrano, J. Ping, M.K. Robinson, A.T.C. Johnson, Genetically Engineered Antibody Functionalized Platinum Nanoparticles Modified CVD-Graphene Nanohybrid Transistor for the Detection of Breast Cancer Biomarker, HER3, *Advanced Materials Interfaces*, 3 (2016) 1600124.

[143] A. Roberts, N. Chauhan, S. Islam, S. Mahari, B. Ghawri, R.K. Gandham, S.S. Majumdar, A. Ghosh, S. Gandhi, Graphene functionalized field-effect transistors for ultrasensitive detection of Japanese encephalitis and Avian influenza virus, *Scientific Reports*, 10 (2020) 14546.

[144] G. Seo, G. Lee, M.J. Kim, S.-H. Baek, M. Choi, K.B. Ku, C.-S. Lee, S. Jun, D. Park, H.G. Kim, S.-J. Kim, J.-O. Lee, B.T. Kim, E.C. Park, S.I. Kim, Rapid Detection of COVID-19 Causative Virus (SARS-CoV-2) in Human Nasopharyngeal Swab Specimens Using Field-Effect Transistor-Based Biosensor, *ACS Nano*, 14 (2020) 5135-5142.

[145] M. Regouc, G. Belge, A. Lorch, K.-P. Dieckmann, M. Pichler, Non-Coding microRNAs as Novel Potential Tumor Markers in Testicular Cancer, *Cancers*, 12 (2020) 749.

[146] C.Y. Goh, C. Wyse, M. Ho, E. O'Beirne, J. Howard, S. Lindsay, P. Kelly, M. Higgins, A. McCann, Exosomes in triple negative breast cancer: Garbage disposals or Trojan horses?, *Cancer Letters*, 473 (2020) 90-97.

[147] N.R. Dalila, M.K.M. Arshad, S.C.B. Gopinath, M.N.M. Nuzaian, M.F.M. Fathil, Molybdenum disulfide—gold nanoparticle nanocomposite in field-effect transistor back-gate for enhanced C-reactive protein detection, *Microchimica Acta*, 187 (2020) 588.

[148] Q. Liu, N. Aroonyadet, Y. Song, X. Wang, X. Cao, Y. Liu, S. Cong, F. Wu, M.E. Thompson, C. Zhou, Highly Sensitive and Quick Detection of Acute Myocardial Infarction Biomarkers Using In2O3 Nanoribbon Biosensors Fabricated Using Shadow Masks, *ACS Nano*, 10 (2016) 10117-10125.

[149] H. Nam, B.-R. Oh, M. Chen, S. Wi, D. Li, K. Kurabayashi, X. Liang, Fabrication and comparison of MoS₂ and WSe₂ field-effect transistor biosensors, *Journal of Vacuum Science & Technology B*, 33 (2015) 06FG01.

[150] B. Ryu, H. Nam, B.-R. Oh, Y. Song, P. Chen, Y. Park, W. Wan, K. Kurabayashi, X. Liang, Cyclewise operation of printed MoS₂ transistor biosensors for rapid biomolecule quantification at femtomolar levels, *ACS sensors*, 2 (2017) 274-281.

[151] M. Chen, H. Nam, H. Rokni, S. Wi, J.S. Yoon, P. Chen, K. Kurabayashi, W. Lu, X. Liang, Nanoimprint-Assisted Shear Exfoliation (NASE) for Producing Multilayer MoS₂ Structures as Field-Effect Transistor Channel Arrays, *ACS Nano*, 9 (2015) 8773-8785.

[152] H. Park, G. Han, S.W. Lee, H. Lee, S.H. Jeong, M. Naqi, A. AlMutairi, Y.J. Kim, J. Lee, W.-j. Kim, Label-free and recalibrated multilayer MoS₂ biosensor for point-of-care diagnostics, *ACS applied materials & interfaces*, 9 (2017) 43490-43497.

[153] L. Wang, Y. Wang, J.I. Wong, T. Palacios, J. Kong, H.Y. Yang, Functionalized MoS₂ nanosheet-based field-effect biosensor for label-free sensitive detection of cancer marker proteins in solution, *Small*, 10 (2014) 1101-1105.

[154] Y. Chen, R. Ren, H. Pu, J. Chang, S. Mao, J. Chen, Field-effect transistor biosensors with two-dimensional black phosphorus nanosheets, *Biosensors and Bioelectronics*, 89 (2017) 505-510.

[155] Y. Gao, Y. Zhou, R. Chandrawati, Metal and Metal Oxide Nanoparticles to Enhance the Performance of Enzyme-Linked Immunosorbent Assay (ELISA), *ACS Applied Nano Materials*, 3 (2019) 1-21.

[156] A.M. Klose, B.L. Miller, A Stable Biotin–Streptavidin Surface Enables Multiplex, Label-Free Protein Detection by Aptamer and Aptamer–Protein Arrays Using Arrayed Imaging Reflectometry, *Sensors*, 20 (2020) 5745.

[157] I. Novodchuk, M. Kayaharman, I.R. Ausri, R. Karimi, X.S. Tang, I.A. Goldthorpe, E. Abdel-Rahman, J. Sanderson, M. Bajcsy, M. Yavuz, An ultrasensitive heart-failure BNP biosensor using B/N co-doped graphene oxide gel FET, *Biosensors and Bioelectronics*, 180 (2021) 113114.

[158] T. Bungon, C. Haslam, S. Damiati, B. O'Driscoll, T. Whitley, P. Davey, G. Siligardi, J. Charmet, S.A. Awan, Graphene FET Sensors for Alzheimer's Disease Protein Biomarker Clusterin Detection, *Front Mol Biosci*, 8 (2021) 651232-651232.

[159] P. Fathi-Hafshejani, N. Azam, L. Wang, M.A. Kuroda, M.C. Hamilton, S. Hasim, M. Mahjouri-Samani, Two-Dimensional-Material-Based Field-Effect Transistor Biosensor for Detecting COVID-19 Virus (SARS-CoV-2), *ACS Nano*, (2021).

[160] M.M. Hossain, B. Shabbir, Y. Wu, W. Yu, V. Krishnamurthi, H. Uddin, N. Mahmood, S. Walia, Q. Bao, T. Alan, S. Mokkapati, Ultrasensitive WSe₂ field-effect transistor-based biosensor for label-free detection of cancer in point-of-care applications, *2D Materials*, (2021).

[161] M. Ma, L. Chao, Y. Zhao, J. Ding, Z. Huang, M. Long, F. Wang, J. Jiang, Z. Liu, High-sensitivity detection of Concanavalin A using MoS₂-based field effect transistor biosensor, *Journal of Physics D: Applied Physics*, 54 (2021) 245401.

[162] S. Schmid, L. Restrepo, G. Huang, C. Joo, G. Maglia, C. Dekker, Single-Molecule Protein Fingerprinting using Nanopores, *Biophysical Journal*, 116 (2019) 316a.

[163] M.-S. Chae, Y.K. Yoo, J. Kim, T.G. Kim, K.S. Hwang, Graphene-based enzyme-modified field-effect transistor biosensor for monitoring drug effects in Alzheimer's disease treatment, *Sensors and Actuators B: Chemical*, 272 (2018) 448-458.

[164] J.W. Park, C. Lee, J. Jang, High-performance field-effect transistor-type glucose biosensor based on nanohybrids of carboxylated polypyrrole nanotube wrapped graphene sheet transducer, *Sensors and Actuators B: Chemical*, 208 (2015) 532-537.

[165] Y.H. Kwak, D.S. Choi, Y.N. Kim, H. Kim, D.H. Yoon, S.-S. Ahn, J.-W. Yang, W.S. Yang, S. Seo, Flexible glucose sensor using CVD-grown graphene-based field effect transistor, *Biosensors and Bioelectronics*, 37 (2012) 82-87.

[166] M. Zhang, C. Liao, C.H. Mak, P. You, C.L. Mak, F. Yan, Highly sensitive glucose sensors based on enzyme-modified whole-graphene solution-gated transistors, *Scientific Reports*, 5 (2015) 8311.

[167] H.W. Lee, D.-H. Kang, J.H. Cho, S. Lee, D.-H. Jun, J.-H. Park, Highly Sensitive and Reusable Membraneless Field-Effect Transistor (FET)-Type Tungsten Diselenide (WSe₂) Biosensors, *ACS Applied Materials & Interfaces*, 10 (2018) 17639-17645.

[168] J. Shan, J. Li, X. Chu, M. Xu, F. Jin, X. Wang, L. Ma, X. Fang, Z. Wei, X. Wang, High sensitivity glucose detection at extremely low concentrations using a MoS₂-based field-effect transistor, *RSC Advances*, 8 (2018) 7942-7948.

[169] Q. Liu, Y. Liu, F. Wu, X. Cao, Z. Li, M. Alharbi, A.N. Abbas, M.R. Amer, C. Zhou, Highly Sensitive and Wearable In₂O₃ Nanoribbon Transistor Biosensors with Integrated On-Chip Gate for Glucose Monitoring in Body Fluids, *ACS Nano*, 12 (2018) 1170-1178.

[170] G.E. Fenoy, W.A. Marmisollé, O. Azzaroni, W. Knoll, Acetylcholine biosensor based on the electrochemical functionalization of graphene field-effect transistors, *Biosensors and Bioelectronics*, 148 (2020) 111796.

[171] E. Danielson, M. Dindo, A.J. Porkovich, P. Kumar, Z. Wang, P. Jain, T. Mete, Z. Ziadi, R. Kikkeri, P. Laurino, M. Sowwan, Non-enzymatic and highly sensitive lactose detection utilizing graphene field-effect transistors, *Biosensors and Bioelectronics*, 165 (2020) 112419.

[172] S. Sheibani, L. Capua, S. Kamaei, S.S.A. Akbari, J. Zhang, H. Guerin, A.M. Ionescu, Extended gate field-effect-transistor for sensing cortisol stress hormone, *Communications Materials*, 2 (2021) 10.

[173] Y. Yang, B. Zeng, Y. Li, H. Liang, Y. Yang, Q. Yuan, Construction of MoS₂ field effect transistor sensor array for the detection of bladder cancer biomarkers, *Science China Chemistry*, 63 (2020) 997-1003.

[174] Y. Chen, R. Ren, H. Pu, X. Guo, J. Chang, G. Zhou, S. Mao, M. Kron, J. Chen, Field-effect transistor biosensor for rapid detection of Ebola antigen, *Scientific reports*, 7 (2017) 1-8.

[175] S. Mansouri Majd, A. Salimi, Ultrasensitive flexible FET-type aptasensor for CA 125 cancer marker detection based on carboxylated multiwalled carbon nanotubes immobilized onto reduced graphene oxide film, *Analytica Chimica Acta*, 1000 (2018) 273-282.

[176] M.M. Nur Nasyifa, A.R. Ruslinda, N.H. Abdul Halim, A.S. Zainol Abidin, F.N. Mohd Faudzi, N.A. Ahmad, Z. Lockman, B. Rezek, A. Kromka, S.C.B. Gopinath, Immuno-probed graphene nanoplatelets on electrolyte-gated field-effect transistor for stable cortisol quantification in serum, *Journal of the Taiwan Institute of Chemical Engineers*, 117 (2020) 10-18.

[177] R.S. Selvarajan, R.A. Rahim, B.Y. Majlis, S.C. Gopinath, A.A. Hamzah, Ultrasensitive and Highly Selective Graphene-Based Field-Effect Transistor Biosensor for Anti-Diuretic Hormone Detection, *Sensors*, 20 (2020) 2642.

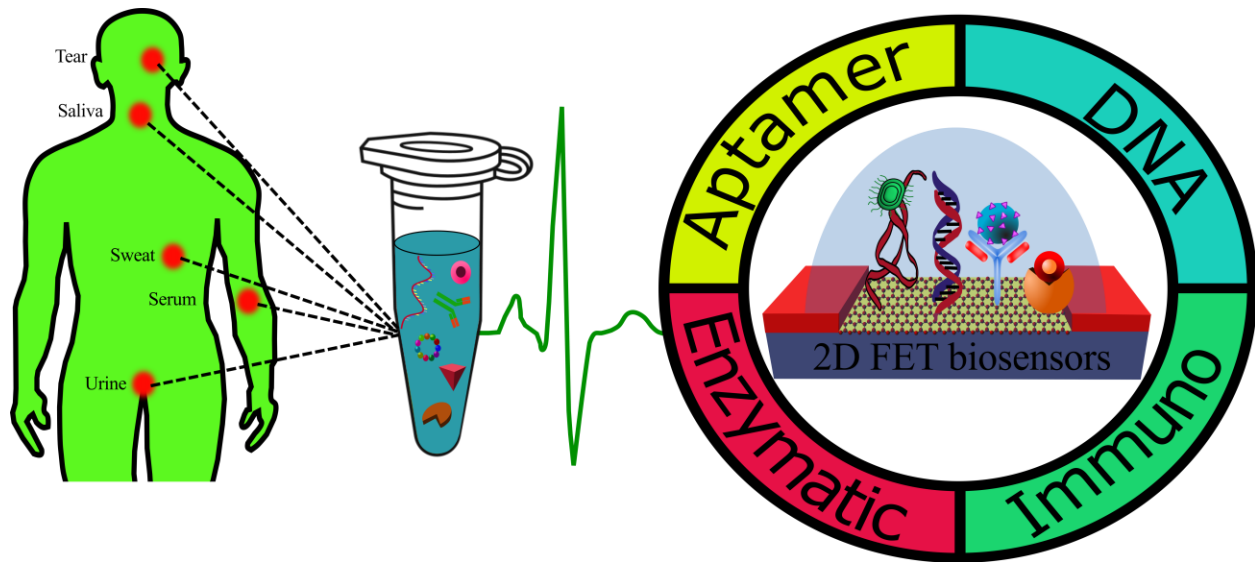
[178] X. Wang, Y. Zhu, T.R. Olsen, N. Sun, W. Zhang, R. Pei, Q. Lin, A graphene aptasensor for biomarker detection in human serum, *Electrochimica Acta*, 290 (2018) 356-363.

[179] M. Sun, C. Zhang, J. Wang, C. Sun, Y. Ji, S. Cheng, H. Liu, Construction of High Stable All-Graphene-Based FETs as Highly Sensitive Dual-Signal miRNA Sensors by a Covalent Layer-by-Layer Assembling Method, *Advanced Electronic Materials*, 6 (2020) 2000731.

[180] M. Shariati, M. Vaezjalali, M. Sadeghi, Ultrasensitive and easily reproducible biosensor based on novel doped MoS₂ nanowires field-effect transistor in label-free approach for detection of hepatitis B virus in blood serum, *Analytica Chimica Acta*, 1156 (2021) 338360.

[181] Y. Zhang, D. Feng, Y. Xu, Z. Yin, W. Dou, U.E. Habiba, C. Pan, Z. Zhang, H. Mou, H. Deng, X. Mi, N. Dai, DNA-based functionalization of two-dimensional MoS₂ FET biosensor for ultrasensitive detection of PSA, *Applied Surface Science*, 548 (2021) 149169.

[182] S. Guo, K. Wu, C. Li, H. Wang, Z. Sun, D. Xi, S. Zhang, W. Ding, M.E. Zaghloul, C. Wang, Integrated contact lens sensor system based on multifunctional ultrathin MoS₂ transistors, *Matter*, 4 (2021) 969-985.



Graphical abstract

Highlights

- The field-effect transistor biosensors (bio-FETs) are presented based on the 2D materials.
- The principle of biosensing in the 2D based bio-FETs are discussed.
- Four categories of the 2D based bio-FETs are introduced depending on their bio-receptor components.
- The performance of the introduced bio-FETs is discussed in bio-medical samples.